8-2021

Electrical characterization of phytoplankton suspensions using impedance spectroscopy.

Margaret R Jett
University of Louisville

ELECTRICAL CHARACTERIZATION OF PHYTOPLANKTON SUSPENSIONS USING IMPEDANCE SPECTROSCOPY

By

Margaret Jett
B.S., University of Louisville, 2018

A Thesis
Submitted to the Faculty of the
Speed School of Engineering of the University of Louisville
in Partial Fulfillment of the Requirements
for the Degree of

Master of Engineering
in Mechanical Engineering

Department of Mechanical Engineering
University of Louisville
Louisville, Kentucky

August 2021

ELECTRICAL CHARACTERIZATION OF PHYTOPLANKTON SUSPENSIONS USING IMPEDANCE SPECTROSCOPY

By

Margaret Jett
B.S., University of Louisville, 2018

A Thesis Approved on

June 30, 2021

By the following Thesis Committee:

Stuart Williams

Ellen Brehob

Cindy Harnett

DEDICATION

I dedicate this thesis to my guinea pigs

Muriel and Cecilia

whose lively conversation helped me work through long nights and tough problems.

ACKNOWLEDGEMENTS

Thank you to my committee for making time for me and taking an interest in my research. Thank you dearly to Professor Williams for the opportunity, the patience, and the guidance he has offered over this period of time. I am very appreciative of my parents for their support, consideration, and enthusiasm as I navigated a new experience like graduate school, and I am also appreciative of Jennifer Zoller for helping with that navigation. Most importantly, I would like to thank my good friend Caroline, whose assistance with editing, writing, and formatting has been invaluable to the completion of this thesis.

ABSTRACT

ELECTRICAL CHARACTERIZATION OF PHYTOPLANKTON SUSPENSIONS USING IMPEDANCE SPECTROSCOPY

Margaret Jett

August 10, 2021

Phytoplankton are closely monitored because of their important environmental role, and the impacts they have on their local ecosystems. Some phytoplankton respond to stress by producing lipids, which can be harvested for biofuels and other chemicals. Microfluidic devices have been important in improving the portability and throughput of phytoplankton characterization methods, increasing their potential for in situ use. This study utilized a small sample of phytoplankton suspended in a stagnant medium and measured the impedance response using a lab-on-chip and impedance analyzer. The individual cell characteristics were derived from the impedance response of the group. The goal was to characterize and differentiate between algae species, as well as healthy and nitrogen deprived cells. The average cytoplasm conductivity was 14.4 mS/m for Chlamydomonas reinhardtii and Selenastrum capricornutum, and not differentiable. The species' average membrane capacitances were differentiable, with S. capricornutum's being 40.6 mF/m^2, and nitrogen-sufficient C. reinhardtii's being 15.5 mF/m^2. Nitrogen-deficient C. reinhardtii's average cytoplasm conductivity and membrane capacitance were 14.1 mS/m and 13.2 mF/m^2.

TABLE OF CONTENTS

LIST OF FIGURES

FIGURE PAGE

CHAPTER I

INTRODUCTION

Phytoplankton are photosynthetic micro-organisms that play an indispensable role in deciphering the health and possible changes in most marine ecosystems. As autotrophs they form the basis of most aquatic food chains, and changes in their population health and productivity can have far reaching impacts (Lindsey & Scott, 2010). Their small size and sensitivity to environmental changes makes them effective eco-signifiers, often times signaling changes in factors such as nutrient density, water oxygen content, toxin presence, and even weather changes. As the primary producers of most marine ecosystems, phytoplankton populations are a food source for a variety of marine life, from microscopic zooplankton to multi-ton whales. Additionally, small fish and invertebrates feed on phytoplankton, and are then eaten by larger predators. As a result, phytoplankton abundance directly affects the abundance of other food sources in each ecosystem, thereby affecting the migration and population health of most marine life. Phytoplankton population changes can also affect other marine life through “blooms”, or periods of explosive phytoplankton population growth. Certain species of phytoplankton produce biotoxins and can cause toxin blooms the kill marine life and contaminate seafood. Even non-toxic blooms can be harmful, as the rapid growth and subsequent death depletes nutrients and oxygen, resulting in dead zones.

Due to their important role as active and reactive agents in marine environments, phytoplankton population changes are monitored by scientists. However, scientists are also researching microalgae use as renewable biofuel and high-value chemical feedstocks (L. Zhu, 2015). When stressed, some phytoplankton species produce lipids, which can then be extracted and converted into a renewable source of biofuel and other high-value chemicals. Microalgae have several advantages over other biofuel sources, such as soybean and oil palm, providing a higher photosynthetic efficiency, faster growth rate, and higher oil content. They also require less water for cultivation (Dismukes, Carrieri, Bennette, Ananyev, & Posewitz, 2008), fixate CO_2 through photosynthesis (B. Wang, Li, Wu, & Lan, 2008), and are diverse and abundant enough that optimal species can be found in almost any environment (Mata, Martins, & Caetano, 2010), including non-arable land (Searchinger et al., 2008). However, the conventional methods used in these processes, such as strain selection, biomass analysis, lipid extraction and analysis, require bulky instruments and labor intensive, high cost, low throughput procedures (Mutanda et al., 2011). Therefore, despite microalgae's advantages over other biofuel feedstocks, production of microalgal based biofuels is not economically viable (Georgianna & Mayfield, 2012).

Improvements in phytoplankton strain selection, biomass analysis, and lipid extraction and analysis are necessary for microalgae-based biofuels, but there is also a need for improvement in phytoplankton characterization technology as a whole. Phytoplankton species differ by location and have specific impacts on their local environments (Maw et al., 2018). Due to the bulk and complexity of most characterization processes, such as microscopy, samples from different locations must be

frozen and transported to labs, a time and money intensive process. This transportation process also has the potential to alter samples, giving inaccurate results during testing. In situ testing, such as on ships, would greatly cut down on the time and cost of phytoplankton characterization. As a result, a variety of quick, easy-to-use, and portable testing methods have been developed that can be used on ships without the need for a specific lab technician.

An obstacle facing the development of quick and easy-to-use phytoplankton characterization methods is the conflict between temporal resolution and spatial resolution (Goda et al., 2012). Temporal and spatial resolution is most often used in image-based analysis methods to describe the trade-off between high-information imaging and high-throughput. Temporal resolution is the discrete resolution of a measurement regarding time. Notably, temporal resolution does not take into account time required for sample preparation or data analysis but do include the trade-off of temporal resolution and computer storage. So, while improvements in speed and ease of sample preparation are still necessary, the temporal resolution of a method describes only the amount of time required to image a sample and store data. Optical microscopy is a widely used method used in several areas of advanced research such as, microelectronics, oceanography, microbiology, and pathology. High information content metrics provided by the optical microscopy imaging are used to characterize microscopic particles, such as emulsions, microorganisms, and cells in particle synthesis, ecosystem monitoring, biofuel formulation, drug discovery, histopathology, and cytology-based diagnostics. There are, additionally, optical nanoscopy methods that can image cellular structures beyond the diffraction limit of light. These high-resolution images are necessary for accurately

identifying and characterizing microscopic particles, but lack temporal resolution, due to the large amounts of digital data created by these high-resolution images. Automated microscopy, which is commonly used for inspecting individual microparticle samples, has a low throughput of 1,000 particles/second. For comparison, high throughput flow analyzers, such as electronic particle counters and flow cytometers, are capable of analyzing around 100,000 particles/second, but lack the spatial resolution to accurately count and characterize microparticles. The result is that, for characterizing a large number of samples, automated microscopes are impractical due to temporal resolution, and high throughput analyzers are impractical due to spatial resolution.

Attempts to improve or work around the spatial and temporal resolution tradeoff have been tested. While high speed cameras have improved the throughput of automated microscopy, they also suffer problems of sacrificing sensitivity for speed, and can require lengthy digital image processing protocols. An alternative to high-definition imaging involves the use of microfluidic devices, or devices that have fluids contained in microchannels, combined with several low-resolution characterization methods, and use the cumulative information to characterize and sort the microparticles (Girault, Beneyton, Amo, & Baret, 2018). These methods often include flow cytometry, side scattering, impedance spectroscopy, fluorescence microscopy, dielectrophoresis, and using hydrodynamic force to separate microparticles with different size and morphologies.

Use of microfluidic devices alongside existing microparticle characterization and sorting apparatus also has the potential for quick and easy in situ applications (Maw et al., 2018). Microfluidic technology has the advantages of needing fewer samples and less reagent, speedier detection, higher efficiency in analysis, miniaturization of volume, and

portability. Microfluidic devices are also easy to fabricate and integrate, so new technology can quickly be developed to suit the needs of different studies.

The purpose of this study is to develop an impedance spectroscopy platform that can characterize stressed, unstressed, and dead phytoplankton cells of different species. Phytoplankton are closely monitored because of their important environmental role, and the impacts they have on their local ecosystems. Some phytoplankton respond to stress by producing lipids, which can be harvested for biofuels and other chemicals. Microfluidic devices have been important in improving the portability and throughput of phytoplankton characterization methods, increasing their potential for in situ use. Impedance spectroscopy has been used to analyze microparticle electrical characteristics, as well as the size and membrane thickness of cells (Coster, Chilcott, & Coster, 1996). However, most devices that utilize impedance spectroscopy arrange the cells in a monolayer or flow channel. The method outlined in this paper differs because a small sample of phytoplankton is suspended in a stagnant medium, and the individual cell characteristics are derived from the impedance response of the group. The advantage of this method is that it is very easy to load samples into and clean the microfluidic device and requires small sample volumes.

CHAPTER II

LITERATURE REVIEW

Phytoplankton and Population Growth

Phytoplankton is a term used to describe a wide variety of photosynthetic micro-organisms that live in watery environments (Lindsey & Scott, 2010). This group is made up of several different microscopic organisms, such as cyanobacteria, diatoms, dinoflagellates, green algae, and coccolithophores. While different phytoplankton species differ in size, shape, and biology, all phytoplankton have chlorophyll to capture sunlight and transform it into chemical energy. As a result, they are all autotrophic, and are therefore the primary producers of all aquatic food webs. As the base of the aquatic food web, their population health directly and indirectly affects the population health of the entire food web (Richardson & Schoeman, 2004). If phytoplankton populations suffer, then organisms that feed on phytoplankton must relocate, rely on different food sources, or reduce their populations. Relocating predators could then impact the food availability in other aquatic ecosystems, leading to increased competition between species or reduced prey populations. On the other hand, reduced predator population could lead to prey overpopulation, or impact other predator populations. As a result, even organisms that do not feed on phytoplankton can be impacted by phytoplankton population health. Phytoplankton populations may also experience periods of rapid growth, or "blooms" (Diaz & Rosenberg, 2008). Some phytoplankton species produce powerful biotoxins, and

as a result they may cause “red tides,” which are harmful algal blooms that can kill marine life and creatures that consume contaminated seafood (Lindsey & Scott, 2010). Phytoplankton blooms are also dangerous because they can deplete environmental resources, and the bacteria that decompose the dead phytoplankton deplete the oxygen in the water, causing a dead zone (Diaz & Rosenberg, 2008). Phytoplankton are also important to the ecosystem because of their impact on carbon sequestration.

Phytoplankton growth on multiple factors, including sunlight, carbon dioxide, and nutrient availability (Behrenfeld et al., 2006). Through photosynthesis, phytoplankton consume carbon dioxide on a similar scale as forests and land plants, transferring about 10 gigatons of carbon from the atmosphere to the deep ocean every year. Phytoplankton consume carbon dioxide and convert it to energy. They are then either consumed by predators or die and sink to the ocean floor (Richardson & Schoeman, 2004). When other creatures consume phytoplankton, the carbon dioxide consumed by the phytoplankton is also consumed and is then transferred to different layers of the ocean as those creatures procreate, excrete waste, and die as well. As a result, even small changes in phytoplankton populations may affect atmospheric carbon dioxide concentrations, which would then impact global surface temperatures. While all phytoplankton species use carbon dioxide and sunlight during photosynthesis, different species have different nutrient requirements (Bopp, Aumont, Cadule, Alvain, & Gehlen, 2005).

There are hundreds of thousands of species of phytoplankton living in Earth’s oceans, and each adapted to particular water conditions (Bopp et al., 2005). As a result, changes in water clarity, nutrient content, and salinity change the species that live in any given place. Ocean changes occur naturally throughout the year, and therefore the

presence of phytoplankton also change naturally (Behrenfeld et al., 2006). Phytoplankton growth varies seasonally because seasonal changes change sunlight availability, water temperature, and nutrient availability brought on by water mixing. However, these seasonal changes also vary geographically. For example, in higher latitudes, winter storms cause water mixing, bringing nutrients up into sunlit surface waters. For this reason, when sunlight increases in spring and summer, phytoplankton blooms peak. However, in subtropical areas, summer causes warm surface water and cold, dense water to separate, causing phytoplankton to use up nutrients and growth to fall off (Diaz & Rosenberg, 2008). While seasonal phytoplankton population changes follow general trends, yearly changes in climate patterns adds a flux to repetitive changes (Lindsey & Scott, 2010).

Yearly phytoplankton population changes are also geographically dependent (Hallegraeff, 2010). The El Nino-Southern Oscillation (ENSO) cycles are responsible for significant changes in typical climate patterns, such as sea surface temperature, wind patterns, and rainfall. El Nino events primarily affect the Pacific Ocean along the equator, but their influence can extend beyond to, for example, the eastern Indian Ocean, the Gulf of Mexico, and the western sub-tropical Atlantic. El Nino events cause easterly trade winds to still or reverse direction. This greatly decreases upwelling which replenishes nutrients necessary for phytoplankton growth, and therefore causes population declines in the equatorial Pacific. The transition between El Nino and its counterpart, La Nina, can also cause a dramatic surge in phytoplankton productivity as upwelling is suddenly renewed. These events cause the most dramatic yearly shifts in phytoplankton

populations. In comparison to ENSO related changes, population changes in mid and high- latitude areas are small.

Periodic population changes as a result of seasonal and yearly changes are monitored and recorded in order to track long term changes in phytoplankton population densities (Lindsey & Scott, 2010). One of the possible influences of climate change is warming surface water leading to increased water column stratification. Increased stratification leads to less water mixing, and therefore nutrients necessary for phytoplankton growth are not recycled. This decrease in available nutrients has the potential to affect phytoplankton population density, but also species composition, as larger species require more nutrients than smaller species. The effects caused by changes in species composition are yet unknown but have the potential to cause a cascade of negative consequences in marine food webs. Small decreases in phytoplankton productivity and larger phytoplankton species populations have already been recorded over the last decade, but the permanence and impact of these changes remains uncertain.

Biofuels

In addition to playing an irreplaceable role in aquatic ecosystems, phytoplankton also have several industrial and manufacturing applications. They have been used for decades as feedstock for applications in cosmetics, pharmacy, and nutrition sectors due to their ability to produce lipids, carbohydrates, and proteins in large amounts (L. Zhu, 2015). For example, they can be used to produce bio-active substances, such as carotenoids, poly saccharides, and β-carotene, and high value molecules such as fatty acids, pigments, and stable isotope biochemicals. They are also increasingly being incorporated in animal feed as a renewable alternative to aquafeed for commercial

poultry and hatcheries. Cyanotech, Seambiotic, Mera Pharma, and FujiChemical all produce and harvest microalgae biomass at a relevant scale for application in cosmetics, nutritious feed, and pharmaceuticals, but there has been a growing interest in microalgae as an alternative fuel source.

Biofuels are renewable energy sources created from organic matter or wastes. Certain species of phytoplankton, when stressed, respond by producing lipids, which can then be used to create a variety of biofuels, such as biodiesel, bioethanol, biogas and biohydrogen (L. Zhu, 2015). Microalgae have several advantages over other biofuel sources, such as soybean and oil palm, including a higher photosynthetic efficiency, faster growth rate, and higher oil content. They also require less water for cultivation (Dismukes et al., 2008), fixate CO_2 through photosynthesis (Wang et al., 2008), and are diverse and abundant enough that optimal species can be found in almost any environment (Mata et al., 2010), including non-arable land and non-fresh water (Searchinger et al., 2008). As a result, they don't threaten farmland like other biofuel sources. However, the conventional methods used in these processes (strain selection, biomass analysis, lipid extraction and analysis, etc.) require high-cost and bulky instruments, and labor intensive and low-throughput procedures (Mutanda et al., 2011). There is no commercial production on a large scale for bulk biofuel application due to the enormous capital and operation investments (L. Zhu, 2015). These high costs have limited bulk scale development, with most optimization efforts based on lab-scale experimental facilities. Therefore, despite microalgae's advantages over other biofuel feedstocks, production of microalgal based biofuels is not economically viable, and this biofuel approach is still in its infancy (Georgianna & Mayfield, 2012).

There has been an increasing interest in microalgae as a source for biofuels, and many studies have focused on culture methods, cultivation engineering, genetic and metabolic engineering, biomass harvest measures, biofuel conversion technologies, cost effectiveness, life cycle assessment, and policy implications (L. Zhu, 2015). An area that has been under examined has been bioprospecting, which encompasses searching and collecting unique microalgae from aquatic environments that can be potentially exploited for the production of high value chemicals and fuels (Mutanda et al., 2011). Microalgal collection is influenced by environmental factors, onsite measuring parameters, aquatic system, and sampling equipment. Since dead and damaged cells may lead to inaccurate test results, the method chosen is crucial to the bioprospecting investigation, and can change depending on each unique situation. Successful biofuel production using microalgae as feedstock requires the identification and collection of suitable microalgae strains, such as hyper-lipid producing and fast-growing strains. Strains should also have low harvest costs, which requires large cell size, high specific gravity relative to the medium, and reliable autoflucculation (Borowitzka, 1997).

Identification Methods

Microalgae cell identification methods are usually microscope-based in labs, such as conventional light microscopy, phase contrast microscopy, fluorescence microscopy, scanning electron microscopy, and transmission electron microscopy for species level identification (Mutanda et al., 2011). Phytoplankton populations in aquatic environments are heterogenous, complex, and vary geographically (J. Wang et al., 2016). As a result, water samples from different geographical locations are collected using ships (Maw et al., 2018). However, since most ships lack the space, technology, and trained workers

required to analyze the samples in situ (in the field), these samples are frozen and transported to a lab, where species are judged and identified by trained personnel using standard microscopy (J. Wang et al., 2016). This method is time intensive, laborious, and inaccurate, requiring long wait times as samples are transported, prepared, and assessed in a lab. Results often differ depending on the operator's experience (J. Wang et al., 2016), and can give misleading results as microalgae change cell size and shape, lose pigmentation and flagella, or die, complicating or making proper identification impossible (Godhe, Anderson, & Rehnstam-Holm, 2002).

Standard microscopy is a widely used method, with uses in microelectronics, food science, energy science, oceanography, archaeology, environmental science, energy science, microbiology, mineralogy, and pathology (Goda et al., 2012). High spatial imaging can characterize microscopic particles such as emulsion, microorganisms, and cells in particle synthesis, ecosystem monitoring, biofuel formulation, drug discovery, histopathology, and cytology-based diagnostics. It describes a variety of modes for imaging cells such as transmitted light, scattered light, fluorescence, and phase contrast (Basiji, Ortyn, Liang, Venkatachalam, & Morissey, 2007). While other microscopy methods, such as confocal microscopy, have superior spatial resolution, standard microscopy is still capable of resolving sub-cellular compartments and structures, making it the standard for clinical cytologic evaluations. There is a fundamental tradeoff between sensitivity and speed (Goda et al., 2012), with standard microscopy achieving high sensitivity at the cost of speed. On the other end of the spectrum is flow cytometry.

Flow cytometry provides rapid data acquisition and is better suited for evaluating pathologies that are present in small numbers (Basiji et al., 2007). However, the data is

only intensity based, and thus is unsuitable for in-depth analysis of morphology, cell type, and phenotypic changes. Flow cytometry is used to analyze individual cells by using a combination of hydrodynamic forces and channels to focus a stream of particles suspended in a fluid. Different channel sizes and configurations can be used to passively sort cells of different morphologies, or in conjunction with an outside analysis method, such as fluorescence microscopy, to quickly characterize individual cells. Flow cytometry is capable of high throughput analysis, but, as a result, struggles to maintain high specifity. Flow cytometry analyses particles in flow, while microscopy analyses particles on slides. Flow cytometry also prioritizes high acquisition rates and fluorescent sensitivity while microscopy emphasizes imaging. As a result, flow cytometry has an analytical throughput of 5,000 cells per second but provides very little subcellular information. In flow cytometry, each detection event is associated with several measurements of fluorescence intensity, and the degree of forward and side scatter of laser light. As a result, rare cell populations can be distinguished by analyzing size, granularity, and fluorescence in a reasonable period of time.

Flow cytometry is commonly used to analyze mixed populations, including phytoplankton populations (Benazzi, Holmes, Sun, Mowlem, & Morgan, 2007). It is a platform that enables rapid, simultaneous, and quantitative analysis of multiple optical properties of individual particles. However, it is a costly instrument and is unable to provide detailed information about species composition, making it difficult to characterize populations. As a result, flow cytometry is often used in conjunction with more traditional techniques, but rarely as a standalone tool. While there is interest in the rapid assay of phytoplankton populations, new flow cytometry-based techniques and the

creation of a database of algae to allow characterization through fingerprinting of algal species have not proven cost effective. One of the issues involved with analyzing phytoplankton populations is the requirement for in situ analysis. In situ use often requires use on ships or other water vessels, making conventional flow cytometry unmanageable due to cost, large size, and significant power requirements (Hashemi, Erickson, Golden, Jackson, & Ligler, 2011). As a result, in situ flow cytometry must be affordable, have a small footprint, and minimal power requirements. However, this flow cytometer must also be able to accommodate a wide variety of particle sizes to accurately characterize marine algae. Attempts have been made to combine the speed of flow cytometry with the sensitivity of standard microscopy, with mixed results.

Automated microscopy is useful for visual inspection of many micro-particles without human intervention (Goda et al., 2012). However, it only has a throughput of a few hundred cells per second, and is therefore unable to evaluate, analyze, and screen large populations with high statistical accuracy in a reasonable period of time. Although high end digital cameras and CMOS are able to perform imaging at a speed approaching 1 million frames per second, they are not suited for high throughput microscopy because their relatively long shutter speed or exposure time causes loss of resolution and motion blur. CMOS cameras are available that can capture greater than a billion pixels per second, corresponding to more than a thousand frames per second for a megapixel image (Schonbrun, Gorthi, & Schaak, 2012). These improved optical components have been combined with microfluidics to implement a multiple field of view imaging flow cytometry. This gives this platform the ability to image multiple channels, thus bypassing the tradeoff between throughput and exposure time. A number of techniques have been

developed to image cells in flow, such as strobed illumination techniques, flying spot scanning, mirror tracking, and slit scanning flow cytometry (Basiji et al., 2007). Challenges associated with imaging cells in flow include achieving sufficient fluorescence sensitivity, producing imagery with high spatial resolution, combining fluorescence imagery with other imaging modes such as brightfield (transmitted light) or darkfield (scattered light), and imaging all the cells in the flow stream. Only recently have advances in CCD camera technology, optical filtration, and digital computing made imaging in flow more practical. For high frame rates, the number of pixels employed must be reduced, losing image resolution and sensitivity (Goda et al., 2012). Additionally, digital imaging cannot be processed in real time due to the massive amount of digital data produced.

Microfluidics

Advances in microfluidic technology have overcome some of the current challenges of high content analysis at population and single cell level that benefit phytoplankton population analysis (Girault, Beneyton, del Amo, & Baret, 2019). Phytoplankton populations have non-homogenous reactions to environmental stimuli. Additionally, evolutionary adaptations to changes in environmental conditions arise from genotypic and phenotypic variations between cells. For this reason, cells within phytoplankton populations experiencing changes to environmental conditions cannot be assumed to also be undergoing the same physiological response. This diversity of physiological responses in cells is hard to detect using classical sampling strategies because they become hidden within the response of the population. Microfluidic technology has the advantage of being able to perform fast cell counts, and differentiate

between organic particles and inorganic, living and dead cells, and different phytoplankton species, while also minimizing space and sample requirements. Microsystems have several benefits such as low unit cost, enhanced flexibility, and improved performance (Benazzi et al., 2007). They are especially suitable for in situ analysis, as problems associated with conventional lab analysis, such as sample degradation, aging, and contamination problems, are eliminated. Flow cytometers have been combined with microfluidic technology to provide a scaled down alternative capable of more detailed in situ analysis of phytoplankton populations. However, their use is still limited by availability, size, cost, complexity, and the need for a specialized operator. Therefore, a major barrier to rapid and cost-efficient phytoplankton analysis is the inability for many traditional methods to be used in situ, such as on ships (Girault et al., 2019). Additionally, optical microscopy characterizes water samples containing a variety of microorganisms and particles using high resolution imaging. High resolution imaging and high throughput are often at odds because high resolution images require slower flow, and longer digital image processing times. Microfluidic technology's miniaturization of nature and equipment presents a solution to these issues. For this reason, a simple, transportable, and affordable microfluidic device would enable quicker and more versatile phytoplankton analysis. Microfluidic devices oftentimes combine multiple methods to more accurately characterize and sort phytoplankton populations.

Some microfluidic devices are used to sort particle samples into subpopulations. These devices are sorted into three categories consisting of passive, active, and hybrid. Passive microfluidic sorting devices use hydrodynamic and Dean forces to sort different morphologies (Girault et al., 2019). The principal of these devices is that particles with

different morphologies and swimming speeds flowing through a channel will naturally disperse into sub-populations as they progress along the channel. Filters, non-linear channels, and chronological channels of decreasing size can be used to increase the specificity of these sorting methods. However, passive sorting methods, while simple and cost-effective, are not suitable for cells of similar morphologies. Active sorting systems are capable of manipulating cells on an individual level, with dielectrophoresis being the most widely used. These sorting methods screen individual cells and, when the sorting condition is fulfilled, a pulse of DC or AC voltage is applied on an electrode on each side of a Y-junction, pulling droplets or cells into a collection stream. A wide range of sorting criteria can be used with this system, and as a result it is suitable for a variety of applications, such as cell identification, growth rate and biological assays. Hybrid systems are defined as sorting systems that can sort numerous events at a specific time but cannot fully work on a single cell or droplet level. These systems generally involve sorting cells by density, compressibility, or lipid content using acoustophoretic or magnetophoric forces. Biochip technology is capable of non-contact manipulation, analysis, and separation of micron-scale particles (Morgan, Holmes, & Green, 2006). Generally, particles flow through microfluidic channels in single file at high-speed using externally generated hydrostatic pressure. Once the particles are focused into a small detection volume, different parameters are measured and analyzed.

An alternative to hydrostatic focusing is using DC fields (Morgan, Holmes, et al., 2006). This technique is dielectrophoresis, or DEP. It relies on dipole forces in non-uniform electric fields to focus the particles independently of the fluid. Dielectric spectroscopy of particles is a method that can non-invasively measure cell parameters

such as size, membrane capacitance, and cytoplasmic conductivity. Microfluidics can be used as a platform for dielectric spectroscopy (Sabuncu, Zhuang, Kolb, & Beskok, 2012). By manipulating minute amounts of liquid, cells can be individually addressed, and external conditions can be adjusted for optimal dielectric measurements, including multiparameter measurements.

Impedance Spectroscopy

Impedance spectroscopy electrokinetic methods are also used to collect cell data, but their sensitivity is limited, and they're labor intensive (Sabuncu et al., 2012). Electrochemical impedance spectroscopy (EIS) studies the system response to the application of an AC signal over a frequency range (Lasia, 2014). An AC electrical current is applied to a specimen and, as the current travels through the specimen, an analyzer measures the impedance response. This response provides information about the specimen's electrochemical and physical structures. It was initially developed to determine double layer capacitance and ac polarography but is now applied for the characterization of electrode processes and complex surfaces. The purpose of analyzing the EIS data is to explain the electrode process and derive its characteristic parameters. While EIS is a sensitive technique, it doesn't directly measure physical phenomena. To interpret impedance spectroscopy, a physio-chemical or measurement model must be used. Measurement modeling involves building a model using mathematical functions to explain the experimental impedance using a best fit method. This method involves using good physical knowledge to model the experimental data using equivalent circuit elements, such as resistors, capacitors, and inductors. The equivalent circuit method is simple and straightforward, but lacks high accuracy, which can cause inconsistency and

degeneracy (Zabara & Ulgut, 2020). Physio-chemical modeling links the measured impedances and the measurement model to physio-chemical parameters of the process (Lasia, 2014). This method has higher accuracy than simply using an equivalent circuit but obtaining the modeling parameters is highly complex and can lead to over-parameterization (Zabara & Ulgut, 2020). Once the circuit model is established, it can then be used to track changes in electrical properties of a sample which indicate changes in the sample.

One use for electrochemical impedance spectroscopy is the characterization of electrical components, such as energy storage systems (ESS) and fuel cells, semiconductors, and super capacitors. This characterization covers a range of energy storage system properties, such as developing equivalent circuit models for different ESS (Zhu, Zhu, & Tatarchuk, 2011), voltage behavior under different loads and discharge conditions (Zabara & Ulgut, 2020), fuel cell health and life cycle (Changjun & Shuhai, 2011), ESS performance changes in response to internal humidity and temperature (Janicka, Mielniczek, Gawel, Darowicki, & Landowska, 2020), efficiency and performance of experimental ESS (Zhu et al., 2011), and ESS material analysis (Meng et al., 2020). The characterization of ESS and fuel cells is important for the development of and operational parameters of ESS and fuel cells (Zhu et al., 2011). There is a push for new improved ESS that are low cost, environmentally friendly, more efficient, rechargeable, or have longer life cycles to replace outdated fuel sources (Nejad, Gladwin, & Stone, 2016). Having a reliable and easy- to-parameterize battery model is important to understanding the performance, voltage behavior, and life cycle of new and existing ESS for industrial applications (Zhu et al., 2011). Impedance spectroscopy is preferred for this

characterization because it is fast, accurate and non-destructive. It is a technique that provides information about the physical properties and time constants of electrochemical processes (Hughes, Allen, & Donne, 2020), including the interfacial process, variation in the internal resistance, state-of-charge, the residual capacity, actual capacity, and state-of-health (Zhu et al., 2011).

The material characterization properties of impedance spectroscopy extend to tissue characterization. Since impedance spectroscopy measures the resistance of an electrical circuit over a range of frequencies, when different tissue types are placed in that circuit, different impedance responses can be specific to that tissue type (Hillary, Brown, Brown, & Balasubramanian, 2020). EIS can detect changes in the shape and structure of cells within a tissue (Brown, Milnes, Abdul, & Tidy, 2005). For example, the "shell sphere model", which describes a spherical cell with a shell-like cell wall and one large cytoplasm in suspension, has been found to be insufficient for describing the dielectric behavior of other cell shapes, such as an ellipsoid cell (Asami & Yonezawa, 1995). As a result, EIS has been used to aid in the diagnosis of prostate (Halter Ryan et al., 2008), bladder (Keshtkar, Salehnia, Keshtkar, & Shokouhi, 2012), skin (Aberg et al., 2004), breast (Stojadinovic et al., 2008), oral (Murdoch et al., 2014), and cervical cancer (Tidy et al., 2013). Cell death characterization is also important to understanding cell biology (Galluzzi et al., 2018); however, traditional death/viability assay are lab intensive and require expensive equipment or reagents (Cummings, Wills, & Schnellmann, 2012). EIS can sense the differences between alive and dead cells and can even differentiate between the different types and modality of death (De Ninno et al., 2020) with the additional positive of being label-free, thus preserving the cells native behavior and therapeutic

potential (Rollo et al., 2017). This sensing ability extends to tissue changes that happen post-mortem, such as detecting the difference between fresh and thawed meat (Tang, Yin, & Lu, 2020). Impedance spectroscopy is also used for quality inspections of meat, fruit, and vegetables in the food industry. This inspection method is preferred because it can be integrated with non-contact measurement methods, is high-throughput, non-destructive, and can obtain bio-impedance spectra to the accuracy of 0.01 S/m, making it preferable for food, medical, and industrial applications.

Studies that use this method are usually aiming to discriminate certain cell types within a group by probing cells at different frequencies (Sabuncu et al., 2012). It is also used to detect the effects of different stimuli by comparing cell impedance at different states. As a result, this method is commonly used in a binary fashion, or for deriving limited information, but the lack of detailed processing steps makes it difficult to apply to a wider context.

Cell Observation Environments

A barrier to observation of phytoplankton populations is that they are microscopic and planktonic, or free floating in a culture medium. As a result, maintaining a controlled environment has complicated observation (Kuntanawat et al., 2014). There are a variety of methods for separating and studying cells from one culture. One technique is the microdroplet based cell encapsulation in oil phase, which separates cells into private compartments. This technique allows the rapid tracking of single cells in parallel, but only in a static mode. It is not very practical for repeated biologic routines and is not cost effective. Cell trapping using suction, channel constriction, or micro cage are most affordable, but it is difficult to design a trap that can handle several different algal

species. One concern for using wells is that microalgae are nonadherent and may freely sink or float depending on cell status and light. These techniques enable tracking the individual growth of several cells, colonies/filaments over a long period of time, as well as algal cell behavior continuously in a culture.

Phytoplankton Species Sampled

Two species of phytoplankton were used, Chlamydomonas reinhardtii and Selenastrum capricornutum. These species are both unicellular green algae that are widely used in experimentation due to their fast growth, short generation time, and easy cultivation (Yang et al., 2018). C. reinhardtii cells are round, single-celled green algae between 10 and 15 microns in diameter (Sasso, Stibor, Mittag, & Grossman, 2018). C. reinhardtii are used as a model for dissecting fundamental processes in biology, because they grow vegetatively as a haploid, so mutant phenotypes are expressed immediately. They also multiply rapidly, with population numbers doubling every eight hours (Harris, 2001). C. reinhardtii are widely used in experimentation to study the biogenesis of cilia and the effects of abnormal cilia in mammalian organisms, because they possess motile cilia that share the same structure and constituent proteins as those of mammals. They are also capable of retaining a functional photosynthetic apparatus in an acetate containing medium, which has enabled the production of non- photosynthetic mutants, and increased understanding of photosynthesis as a process (Sasso et al., 2018). When stressed through nitrogen deprivation, C. reinhardtii react by storing neutral lipids in lipid bodies, by sacrificing biomass (Yang et al., 2018).

Selenastrum capricornutum are sickle shaped, unicellular, fresh water green algae that are between 4 to 7 microns long (Yamagishi, Yamaguchi, Suzuki, Horie, &

Tatarazako, 2017). S. capricornutum has a high growth rate and proliferates most commonly by forming four autospores through multiple fission after two nuclear divisions. However, it is capable of other reproductive patterns, such as binary fission and eight autospore multiple fission, depending on culture conditions and the presence of toxicants. S. capricornutum is commonly used as a bioindicator for the presence of waterborne contaminants (Newsted, 2004). Due to their small size, and relatively large surface area, they reach steady state quickly when contaminates are introduced, and thus produce toxicity test results quickly. Also, unlike bacteria, they don't compete once the nutrient medium is depleted, so they can be used for growth inhibition toxicity tests in pure water (Ivanova & Groudeva, 2006).

Relevance to Work Herein

The purpose of this study was to determine whether an impedance spectroscopy platform can be used to differentiate between healthy and nitrogen deprived cells, as well as cells of different phytoplankton species. These species were chosen because of their quick growth rates, extensive experimental use, and distinct cell size and formations. Impedance spectroscopy has been used to characterize the impedance response of circular cells with a capacitive membrane and resistive cytoplasm in suspensions for D.C., and A.C. cases (Coster et al., 1996), a model that closely resembles C. reinhardtii. Impedance spectroscopy has also been used to estimate cell size and membrane thickness to the resolution of nanometers, and has characterized the membrane capacitance of human, calf, dog, rabbit, chicken, and turtle blood cells, as well as Arbacia, Asterias, and frog eggs. Impedance spectroscopy can differentiate different cells in suspension by their size and impedance response, as well as biomass. Therefore, two species of different size and

cell formation should have two distinct cell responses. Additionally, since C. reinhardtii produces lipids, and reduces biomass in response to nitrogen deprivation, stressed and unstressed cells should also have two distinct impedance responses.

CHAPTER III

METHODS AND MATERIALS

Instrumentation

The impedance analyzer used was the Hewlett-Packard 4294A Precision Impedance Analyzer (Figure 1) and the probe used was the 42941A Impedance Probe Kit (Figure 2). The ECIS Cultureware ™ chip, Model Number 8W20idf PET (Figure 3), was a chip with eight wells containing gold film electrodes delineated with an insulating film. The well top was made from polystyrene. Each electrode had inter-digitated fingers, with a total area of 3.985 mm^2, covering most of the well bottom. Each well substrate area was 0.8 cm^2, and a maximum volume of 600 µL. Typically these chips would be used to measure confluent cell layers on the bottom of the well. For these cases, approximately 6,000 to 8,000 cells would be measured by the electrodes.

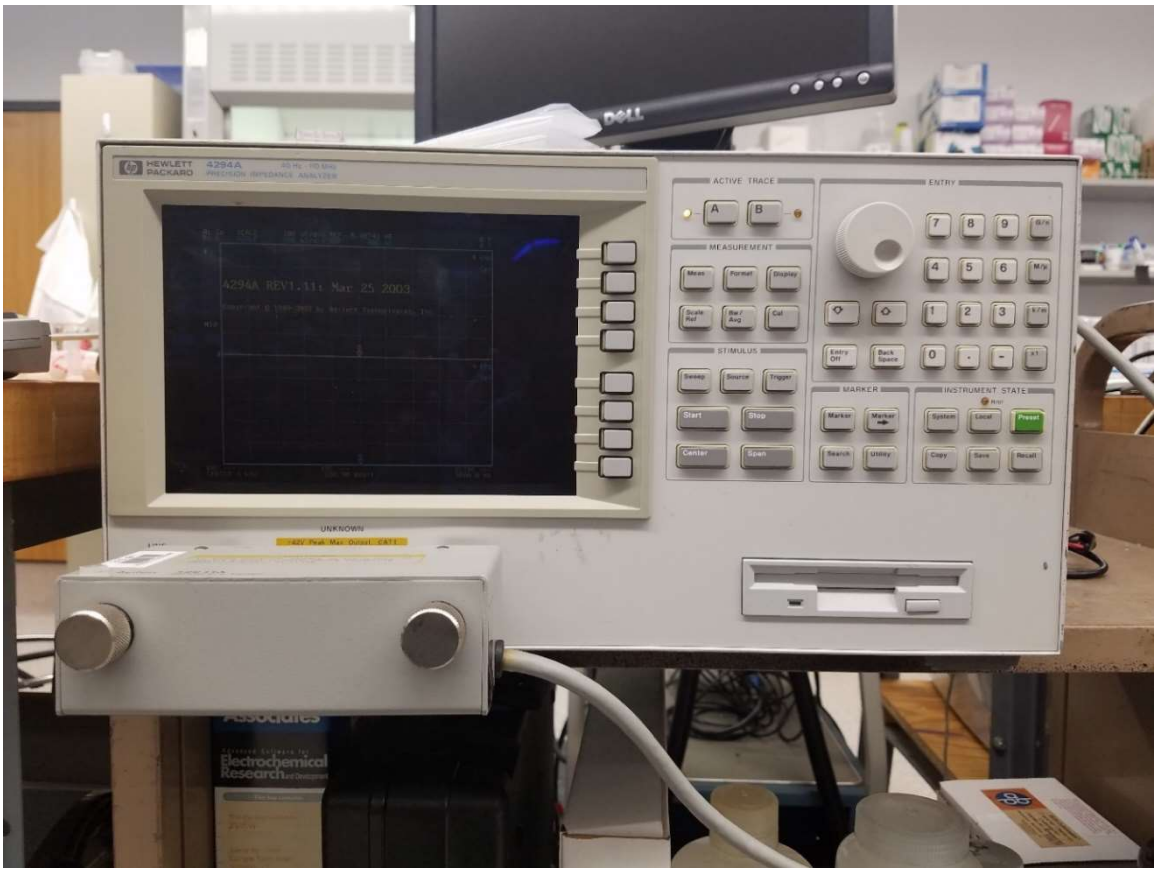

Figure 1. Front view image of the Hewlett-Packard 4294A Precision Impedance Analyzer.

Figure 2. Image of the 42941A Impedance Probe attached to the fabricated chip holder

This chip was chosen because it was designed to monitor large numbers of cells, and the well depth and electrodes were such that each well could be loaded and unloaded using a pipette, making it straightforward to use. The ability to monitor a large number of cells minimizes the impedance fluctuations caused by cell micromotion. Phytoplankton can move, and oftentimes sink to the bottom of media if left alone. Since this experiment specifically tests phytoplankton suspended in media, these movements can impact impedance measurements and obscure subtle changes due to environmental conditions. Therefore, for accurate results these fluctuations must be minimized.

While this chip was straightforward to use, it required a unique holder to be used with the impedance analyzer and probe.

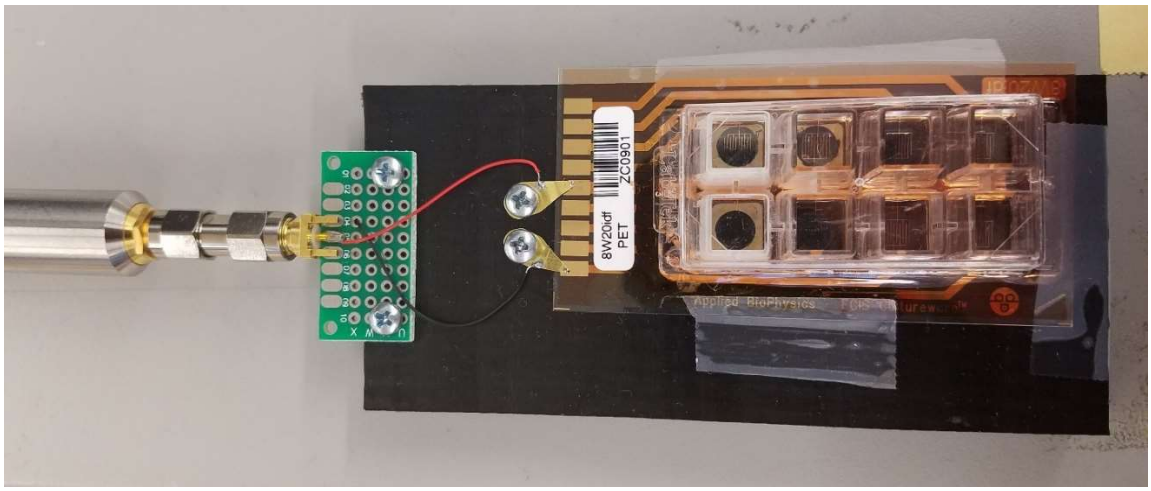

Figure 3. The ECIS Cultureware ™, Model Number 8W20idf PET, chip connected to the probe using custom interface.

The chip's eight wells were independently addressable and were hooked up to the impedance analyzer via copper bonding pads. The electrode's bonding pads were lined in a row, along with a grounding connection, on one side of the chip. A custom interface was developed that would connect the impedance analyzer with the chip (Figure 3). This

chip holder was fabricated with two metal digit connectors using wires and a small solderable perf board. These electronic components were mounted onto a wood block. The chip would be place onto the chip holder, and the chip holder metal digits would be used to connect to different wells and the ground via the copper film. This chip holder was preferred because of the ease of changing between wells and chips, as opposed to the alternative of soldering the impedance connector directly to the chip.

The impedance analyzer and probe used was the Hewlett-Packard 4294A Precision Impedance Analyzer and the 42941A Impedance Probe Kit. The purpose of the impedance analyzer for this experiment was to apply an AC sinusoidal electrical signal over a frequency range through the probe to a test subject, in this case the sample in the chip well. First, the probe was attached to the analyzer, the machine was turned on, and the probe was selected for calibration on the impedance analyzer menu screen. The impedance analyzer settings controlled the response measured, sweep type, frequency range, bandwidth, and signal source strength. The impedance analyzer measured and reported the impedance magnitude and phase. The signal sweep was a logarithmic sweep over the frequency range 40 Hz to 10 MHz. The logarithmic sweep was chosen because it spends equal time in each octave, which gives lower frequency wavelengths more time to resolve. Three bandwidths were used, and the signal source strength was 10 mV.

These settings remained the same for all trials. Next, the probe was calibrated. The purpose of this calibration was to correct for the impedance fluctuations caused by running the electrical signal through the probe and analyzer, so that they could be adjusted by the analyzer for the actual experiment. This is similar to taring a scale before weighing something. It was accomplished by running an electrical signal from the

analyzer through the probe when the circuit was open and shorted. The open circuit was achieved by running an electrical signal through the probe when nothing was attached to it. The short circuit was achieved by attaching a circular piece of wire to the end of the probe so that it connected to itself and running another electrical signal through it. After this, the impedance analyzer and probe would be ready for the experiments.

The impedance analyzer measured the impedance response of the sample and chip and displayed the result as a graph on the screen. This graph plotted the change in impedance magnitude and phase over the frequency range. This information was analyzed in MATLAB as outlined below.

Procedures

This experiment compared the impedance response between stressed and unstressed Chlamydomonas reinhardtii and compared the impedance response between unstressed Chlamydomonas reinhardtii and Selenastrum capricornutum. The phytoplankton were ordered from Carolina Biological Supply (CBS). Their recommended culturing conditions are listed in Table 1.

Table 1

Optimal Culturing Conditions for Experimental Phytoplankton Taxon

Taxon	Source	Cell Size	Culturing Conditions			
		Diameter (μm)	Temperature (°C)	Light/ Dark (hrs)	Growth Media	Incubator
Chlamydomonas reinhardtii	CBS	10-12	22	12hr/ 12hr 5-6 watts	Alga-Gro, BBM, Soil Extract + Spring Water	Percival
Selenastrum capricornutum	CBS	5-7	22	12hr/ 12hr 5-6 watts	Alga-Gro, BBM	Percival

The phytoplankton were first cultured in Alga-Gro (AG) or soil extract-spring water (SoilXSW), and once they had acclimated to the culture conditions in the lab, they were transferred to Bold's Basal Medium. The cells were left to culture for several days to weeks, until the cells grew to a dense stable population of approximately 10^9 cells/mL. The cells were then pelletized by centrifugation at 1500 rpm, and then transferred to either nitrogen rich (N+) or nitrogen poor (N-)

BBM five days before experimentation. The N- stressed cells were stained by adding 5-10 µL of Bodipy 5/515 stock solution (Invitrogen, Grand Island, NY) dissolved in dimethyl sulfoxide at 0.5 mg/mL. Cells were allowed to stain for 30 minutes, then examined at 400X magnification to confirm the presence of lipid bodies using a fluorescence Zeiss Axioplan microscope (Excitation: 470/40X, dichromatic mirror: 495, emission:525/50m). Cells grown in N+ medium were also stained and checked to ensure no lipid production.

Once the phytoplankton populations plateaued, they were transported to the lab. The impedance spectrometer would display noise when the cell density exceeded 10^6 cells/mL, so the cell density had to be found and diluted for more accurate results. Additionally, the ideal conductivity for the phytoplankton suspended in media was between 10 and 20 µS/cm. The growth medium greatly exceeded this range, so the phytoplankton were gradually resuspended in less conductive solutions of potassium chloride, deionized water, and glucose (85 g/L). First, 1.5 mL microcentrifuge tubes were filled with the original cell culture. They were spun down using an Eppendorf Centrifuge 5415 C (Figure 6) at 8000 rpm for 15 minutes, or until the samples had sufficiently pelletized. Once the phytoplankton were pelletized, the supernatant was disposed of into a waste fluid container. Then, the pellets were dislodged from the tube wall using 1.5 mL of a 40% KCl solution (100 µS/cm), checked for licing, and re-spun under the same conditions. Once repelletized, the pellets were dislodged with 20% KCl solution (40 µS/cm). This method was repeated two more times with 5% KCl (10 µS/cm), and then the conductivity was measured using a conductivity meter.

Figure 4. Leitz Wetzlar microscope.

Once the solution conductivity was within 10 to 20 µS/cm, the cell density was found. A sample of the phytoplankton was loaded into a Palmer Counting

Cell (Figure 5), and the cell was covered with a slide cover. The cell was placed under a Leitz Wetzlar microscope (Figure 4), and focused. The phytoplankton cells in view were then counted, the counting cell was moved, focused, and the cells were counted again. This was repeated eight times. The cell density was then calculated using

$$\frac{\text{Cells}}{\text{mL}} = \frac{\text{C}(1000\text{mm}^3)}{\text{A} * \text{D} * \text{F}} \quad (1)$$

where C is the total number of cells counted, A is the areas of Leitz microscope at 400X magnification, which in this case was 0.16982 mm^2, D is the depth of the Palmer cell, in this case 0.4 mm, and F is the number of fields counted, in this case eight. If the cell density was higher than 10^6, it was lowered by adding 5% KCl to the phytoplankton solution. The conductivity was then re-tested, and the diluted phytoplankton solution was loaded into the Palmer Counting Cell, and the process was repeated until the phytoplankton solution was within the necessary range for cell density and conductivity.

Figure 5. Palmer Counting Cell.

Figure 6. Centrifuge 5415 C.

Once the phytoplankton test samples were within the appropriate conductivity and cell density ranges, they could be tested using the impedance analyzer. First, the chip was placed into the holder. A well was chosen for analysis by moving one of the chip holder's metal arms onto the bonding pad connecting to a well, moving the other arm onto the ground connection, and securing both by tightening a screw that attached them to the holder base. Once the well was connected to the impedance analyzer, a 200 µL sample was pipetted into the well. Then, the "Trigger" button was pressed, and the "hold" option was selected to stop the analyzer from sensing. When the analyzer had stopped sensing, the chip holder and chip were connected to the probe. Then the "Bw/Avg" button was pressed, and "Averaging Restart" and "Averaging ON" were chosen from the menu items. Then "Trigger" button was selected again, the "Number of groups" was selected, and 3 was entered on the keypad and entered by hitting the "x" keypad button. This meant the analyzer would take three scans and average them. Once the results are displayed on the screen, the view can be adjusted by pressing the "Scale/ref" button and can automatically adjusted for easiest viewing using the "Autoscale" menu item.

After the measurement was complete, they were saved onto a floppy disk. The "Save" button was pressed, and floppy was chosen under the "Store dev" option. Under the "Data" menu item, "ASCII" was chosen as the export data type. The save file was named using a keyboard. Once the measurement was saved, the sample was pipetted out of the well, the chip was removed from the chip holder, and the well was rinsed with DI water and dried with a blast from a nitrogen hose. Only DI water was used to clean the wells, because other cleaning option such as acetone and ethanol were too harsh for the well's delicate substrate layer. With the well clean and dry, the chip was placed back into

the chip, another 200 µL was pippeted into the well. Another measurement was then taken by pressing the "Trigger" button, selecting "Number of groups", and dictating those three measurements be taken and averaged. When completed, this average was saved onto the same floppy disk. Once the data was transferred from the floppy disk to the computer, it was analyzed in MATLAB.

Theoretical Concept

The calculations were based off the method used in "Evaluation of single cell electrical parameters from bioimpedance cells suspension" (Das, Kamil, Biswas, & Das, 2014), which derived single cell electrical characteristics from the impedance response of cells suspended in a medium. Figure 7 is a flow chart describing the calculation process, including experimental inputs and calculated values.

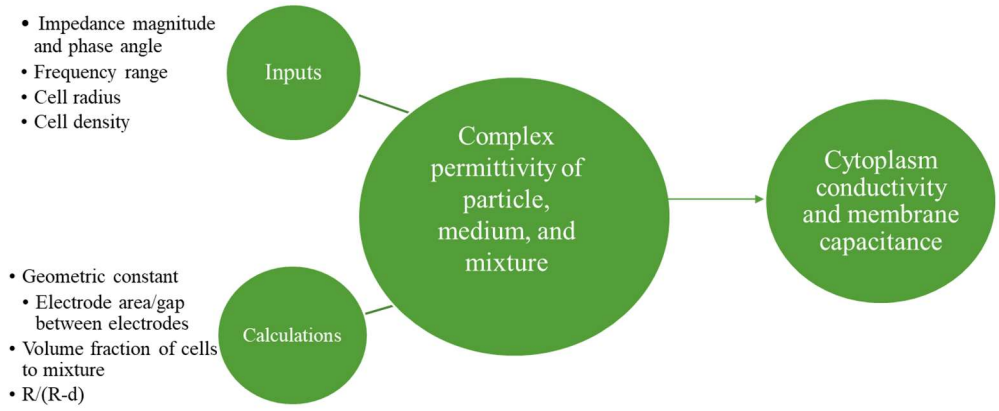

Figure 7. Flow chart describing the process of calculating outputs from the experimental and calculated inputs.

The basic principle of impedance is based on Ohm's law, which states that an electric potential, $V(j\omega)$, can be measured by applying an electric current through a material, where $\omega = 2\pi f$ is the angular frequency and $j^2 = -1$. If small

AC voltages are used over a range of frequencies as an excitation signal, a group of cells in suspension would oppose the applied electric current, I(jω), generating impedance $\tilde{Z}(j\omega)$. This impedance $\tilde{Z}(j\omega)$ is expressed as

$$\tilde{Z}(j\omega) = {}^{V(j\omega)}\Big/_{I(j\omega)} = \tilde{Z}_{\mathrm{RE}} + j\tilde{Z}_{\mathrm{IM}} \tag{2}$$

where $\tilde{Z}_{RE}$, resistance, and $\tilde{Z}_{IM}$, reactance, are the real and imaginary parts of the complex impedance, respectively. Moreover, the complex impedance is a function of complex permittivity, $\tilde{\varepsilon}$, and conductivity, σ, of the cell's cytoplasm and membrane. Therefore, the impedance response can be used to calculate the cytoplasm conductivity and membrane capacitance, which can theoretically be used to differentiate species and high-lipid cells from low-lipid cells.

For diluted cells in suspension, the total impedance of the system is described by Maxwell's mixture theory (Maxwell, 1954). The equivalent complex permittivity of the mixture is related to the total impedance of the mixture by (Sun & Morgan, 2010)

$$\tilde{Z}_{\mathrm{mix}} = \frac{1}{j\omega\tilde{\varepsilon}_{\mathrm{mix}}G} \tag{3}$$

where G is the electrode's geometric constant, which is the ratio of the electrode area to the gap between the electrodes, and

$$\tilde{\varepsilon}_{\mathrm{mix}} = \tilde{\varepsilon}_{\mathrm{m}}\frac{1 + 2\varphi\tilde{f}_{\mathrm{cm}}}{1 - \varphi\tilde{f}_{\mathrm{cm}}} \tag{4}$$

where φ is the volume fraction (ratio of the particle volume to the suspending medium volume), and $\tilde{f}_{cm}$ is the complex Clausius-Mossotti factor, given by

$$\tilde{f}_{\mathrm{cm}} = \frac{\tilde{\varepsilon}_{\mathrm{p}} - \tilde{\varepsilon}_{\mathrm{m}}}{\tilde{\varepsilon}_{\mathrm{p}} + 2\tilde{\varepsilon}_{\mathrm{m}}} \tag{5}$$

where $\tilde{\varepsilon}_{\mathrm{p}}$ and $\tilde{\varepsilon}_{\mathrm{m}}$ are the complex permittivity of the particle/cell and medium, given by

$$\tilde{\varepsilon} = \varepsilon - \mathrm{j}\frac{\sigma}{\omega} \tag{6}$$

where ε is the permittivity and σ is the conductivity.

It is noted that Maxwell mixture theory is valid for low volume fractions ($\varphi < 10\%$) i.e., the volume of the cells suspended in the media is below <10% of the total mixture volume.

$$1 - \varphi = \left(\frac{\tilde{\varepsilon}_{\mathrm{mix}} - \tilde{\varepsilon}_{p}}{\tilde{\varepsilon}_{\mathrm{m}} - \tilde{\varepsilon}_{p}}\right)\left(\frac{\tilde{\varepsilon}_{\mathrm{m}}}{\tilde{\varepsilon}_{\mathrm{mix}}}\right)^{1/3} \tag{7}$$

In impedance spectroscopy-based analysis, it's common to obtain the dielectric properties of the single cell (i.e., cytoplasm conductivity, σ_{cyt}, membrane conductance, σ_{mem}, and specific membrane capacitance, $\mathrm{C}_{\mathrm{mem}}$) from suspension by utilizing the single shell model to represent single cells and Maxwell mixture theory (Morgan, Sun, Holmes, Gawad, & Green, 2006).

In single shell model (Figure 8a), the complex permittivity of the cell is given by (Morgan, Sun, et al., 2006; Sun & Morgan, 2010)

$$\tilde{\varepsilon}_{p} = \tilde{\varepsilon}_{mem}\frac{\gamma^3 + 2\left(\frac{\tilde{\varepsilon}_{\mathrm{cyt}} - \tilde{\varepsilon}_{\mathrm{mem}}}{\tilde{\varepsilon}_{\mathrm{cyt}} + 2\tilde{\varepsilon}_{\mathrm{mem}}}\right)}{\gamma^3 - \left(\frac{\tilde{\varepsilon}_{\mathrm{cyt}} - \tilde{\varepsilon}_{\mathrm{mem}}}{\tilde{\varepsilon}_{\mathrm{cyt}} + 2\tilde{\varepsilon}_{\mathrm{mem}}}\right)} \tag{8}$$

where $\gamma = R/(R - d)$, R is the radius of the cell, d is the thickness of the cell membrane (Figure 8) and $\tilde{\varepsilon}_{cyt}$ and $\tilde{\varepsilon}_{mem}$ are the complex permittivities of the cytoplasm and membrane, respectively.

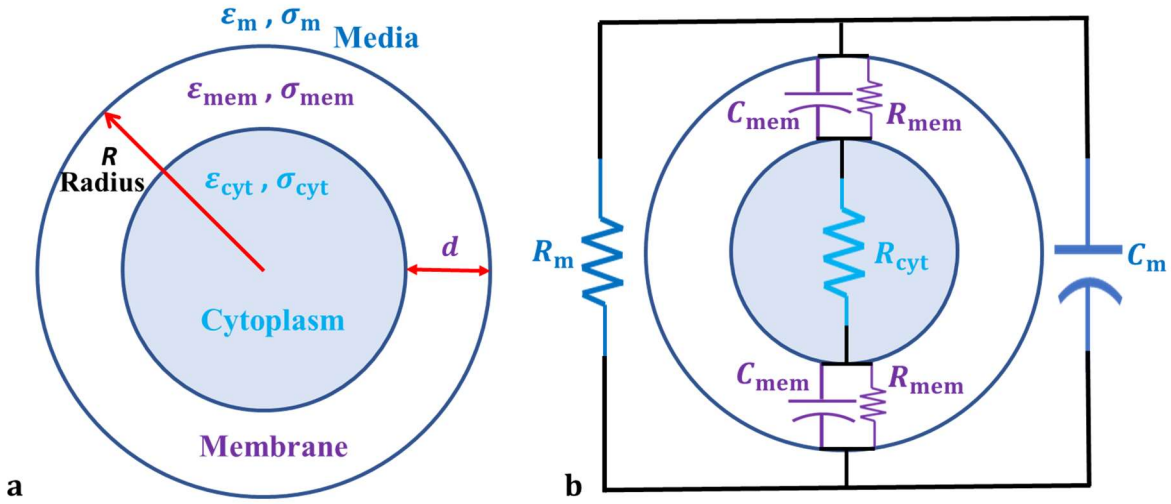

Figure 8. Schematic diagram of (**a**) single-shell model of cells in suspension (**b**) simplified equivalent electrical circuit model (ECM) of single cells in suspension neglecting the double layer electrical components.

The equivalent electrical model of cells suspended in aqueous media is used to simplify the mathematical expressions used to extract the single cell properties from the measured complex impedance. By stating that $\tilde{\varepsilon}_{cyt} = -j\,\sigma_{cyt}/\boldsymbol{\omega}$ and $\tilde{\varepsilon}_{mem} = \varepsilon$, then Equation 7 can be simplified to (Das et al., 2014)

$$\tilde{\varepsilon}_p = \varepsilon \frac{\gamma^3 + 2\left(\frac{-j\,\sigma_{cyt}/\boldsymbol{\omega} - \varepsilon}{2\varepsilon - -j\,\sigma_{cyt}/\boldsymbol{\omega}}\right)}{\gamma^3 - \left(\frac{-j\,\sigma_{cyt}/\boldsymbol{\omega} - \varepsilon}{2\varepsilon - -j\,\sigma_{cyt}/\boldsymbol{\omega}}\right)} \left(\frac{\mathrm{Re}[\tilde{\varepsilon}_p] + j\,\mathrm{Im}[\tilde{\varepsilon}_p]}{\varepsilon}\right) \tag{9}$$

which can be simplified to

$$\tilde{\varepsilon}_p = \left(\frac{2b\varepsilon^2 + a(\,\sigma_{cyt}/\boldsymbol{\omega})^2}{b^2\varepsilon^2 + (\,\sigma_{cyt}/\boldsymbol{\omega})^2}\right) + j\left(\frac{\varepsilon\,\sigma_{cyt}/\boldsymbol{\omega}(2-ab)}{b^2\varepsilon^2 + (\,\sigma_{cyt}/\boldsymbol{\omega})^2}\right), \tag{10}$$

where $a = \left\lfloor\frac{\gamma^3+2}{\gamma^3-1}\right\rfloor$ and $b = \left\lfloor\frac{2\gamma^3+1}{\gamma^3-1}\right\rfloor$.

A quadratic equation can be obtained by dividing the real and imaginary parts by $\tilde{\varepsilon}_p$ in Equation 9:

$$\frac{a}{\omega}(\,\sigma_{cyt}/\varepsilon)^2 - k(2-ab)(\,\sigma_{cyt}/\varepsilon) + +2b\omega = 0, \tag{11}$$

where $k = \left\lfloor\frac{\mathrm{Re}[\tilde{\varepsilon}_p]}{\mathrm{Im}[\tilde{\varepsilon}_p]}\right\rfloor$. By assuming that $L = \sigma_{cyt}/\varepsilon$ and solving the imaginary part of Equation 9 for ε, the extracted permittivity of a single cell from the complex becomes

$$\varepsilon = \left(\frac{b^2 + (L/\omega)^2}{(L/\omega)(2-ab)}\right)\mathrm{Im}[\tilde{\varepsilon}_p] \tag{12}$$

From Equation 10, L can be calculated and used to calculate ε; after that σ_{cyt} can be calculated.

As shown in Figure 8b, the total impedance of the mixture consists of the impedance of the medium represented by the parallel resistance and capacitance of the aqueous media, and the impedance of the single cells. The impedance of single cell is simplified to include the resistance of the cytoplasm in series with the membrane impedance represented as resistance and capacitance which acts as a dielectric material which can be measured at higher frequencies where it plays a major role in determining the impedance of cells (Foster & Schwan, 1989). Hence, the values of the frequency dependent cell parameters such as specific

membrane capacitance can be determined by the volume fraction, conductive and dielectric properties of both cell and medium, as well as the cell size and geometric constant of the electrodes used for measurements (Morgan, Holmes, et al., 2006; Sun & Morgan, 2010), such that the capacitance of the cell membrane may be calculated using

$$C_{mem}(\omega) = \frac{9\varphi R\varepsilon}{4d} G \tag{13}$$

CHAPTER IV

RESULTS AND DISCUSSION

The continued push for improving phytoplankton research equipment has led to the integration of microfluidics with traditional phytoplankton characterization methods. This study attempts to further broaden this field by demonstrating the viability of microfluidic impedance spectroscopy in phytoplankton characterization. While many past studies involved the use of impedance spectroscopy in a variety of research and industrial uses, research that focused on phytoplankton characterization used specially fabricated chips, cell labelling, or the combination of several different characterization procedures. These factors complicated the experiment set-up and results analyzation, making them inaccessible for in situ use. This study demonstrated that a pre-existing chip and machine, in conjunction with a fabricated chip platform, can measure the electrical characteristics of phytoplankton cells in suspension with enough precision to identify different samples containing different species and differentiate between healthy and nitrogen-deprived cells.

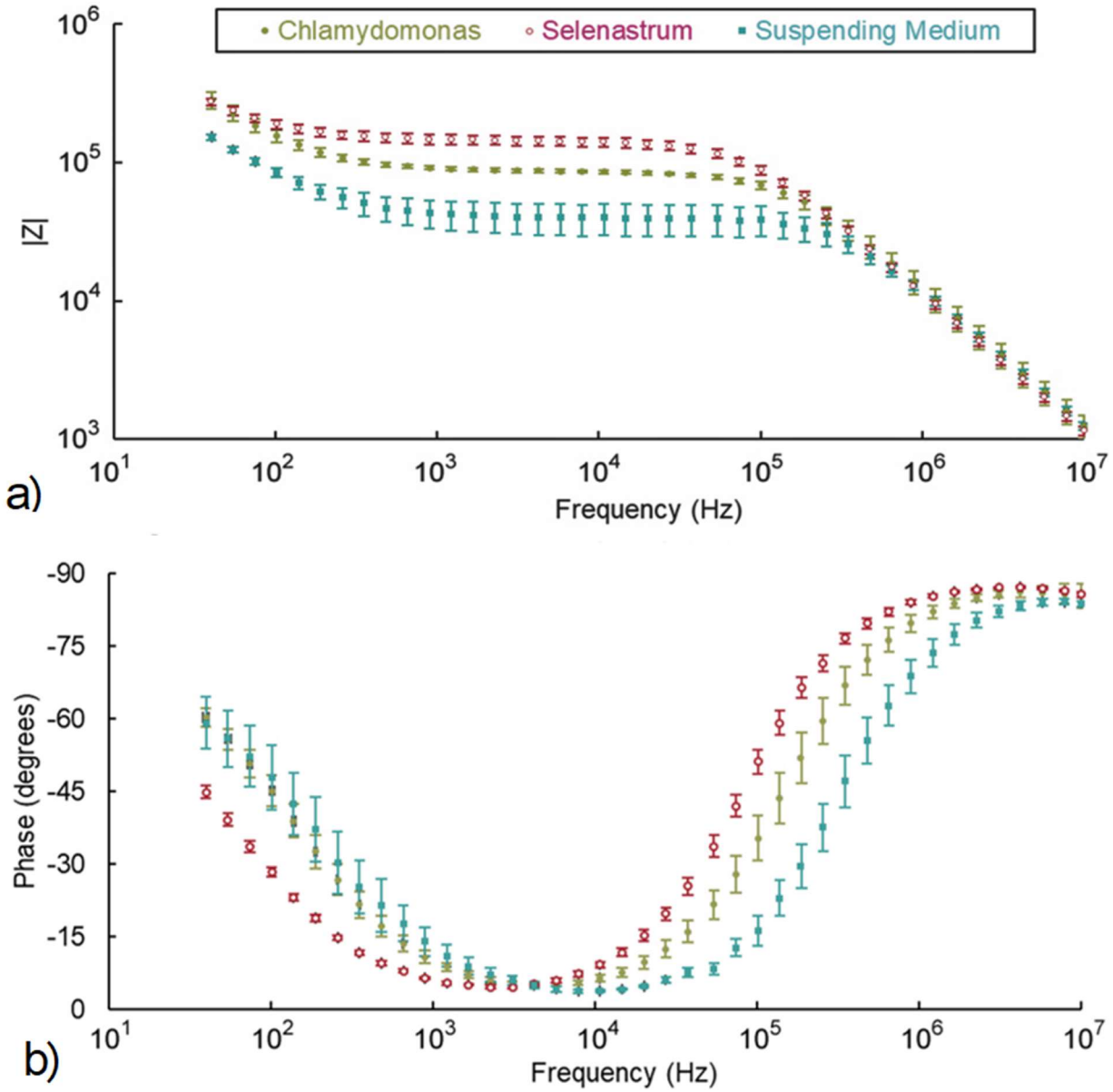

Figure 9. Average and standard deviation of impedance magnitude and phase angle for C. reinhardtii, S. capricornutum, and conducting media.

Figure 9 displays the impedance magnitude and phase angle of the electrolyte medium, and medium with Chlamydomonas reinhardtii and Selenastrum capricornutum. As can be seen, the addition of cells to the medium increased the impedance magnitude and shifted the phase angle. This reflects that the addition of cells in suspension within an

electrolyte solution has a significant enough effect that it can alter the impedance output over a range of frequencies. As can also be seen in Figure 9, the curves all resemble each other in shape, and the impedance magnitude curves converge as the frequency surpasses 200 kHz. This is a result of the Nernst-Planck-Poisson electro-diffusion theory, and the curves behavior can be broken down into different dispersions that occur at different frequencies (Coster et al., 1996). Low frequencies characterize the α dispersion, with the AC electrical field establishing ionic concentrations and gradients that affect positive and negative ions differently. As a result, the diffusion currents can be much larger and out of phase with the field driven current. This has an effect similar to a very large capacitor. As the frequency increases, the time for the AC ionic concentrations and gradients decreases, which in turn causes the capacitive effect to also decrease. This is the β dispersion, and it is characterized by interfacial polarization, or the polarization resulting from the boundary layers within the electrolyte solution, such as the electrolyte/electrode boundary, electrolyte/membrane boundary, and membrane/cytoplasm boundary. As frequency increases, the α and β dispersions result in graphs like those in Figure 9.

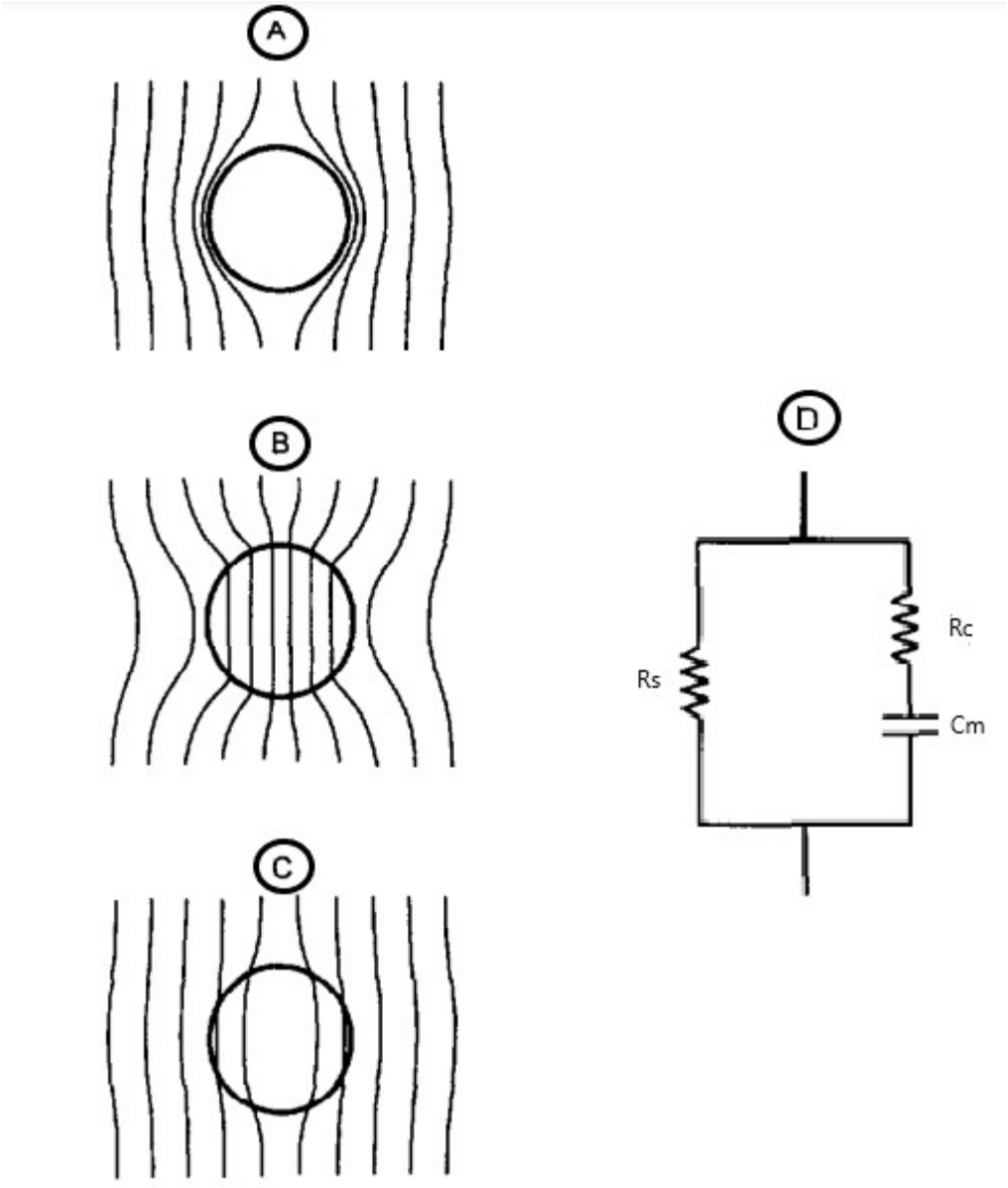

Figure 10. Current flow across a perfectly spherical cell wrapped in a thin membrane a) low frequencies, b) moderate frequencies, c) sufficiently high frequencies, as well as d) the equivalent circuit for this model, where R_s is the conducting medium resistance, R_c is the cytoplasm resistance, and C_m is the membrane capacitance. Modified from Coster et al. (1996).

With this understanding of dispersions, the frequencies at which electrical characteristics would be most prominent or reliable could be chosen. For example, at low frequencies, the membrane effectively insulates the cytoplasm, causing the current to

only flow around the cell (Figure 10a). As the frequency increases, the conductivity of the membrane increases as the complex conductivity of the cytoplasm approaches that of the bulk solution. This ratio increases as the frequency increases, subsequently allowing the current to flow across the membrane and through the cytoplasm (Figure 10b). At sufficiently high frequencies, the ratio of the complex conductivities approaches that of the permittivity of the cytoplasm to the bulk solution, causing unity (Figure 10c). When comparing this cell behavior to the dispersions mentioned above, the appropriate frequency range can be chosen for analysis. This range must be large enough such that both the membrane capacitance, and cytoplasm resistance (or the reactive and resistive components of the impedance) were sensed by the machine, but small enough to minimize the effects of diffusion fields as possible. As a result, to characterize the membrane capacitance and cytoplasm conductivity of cells in suspension, the appropriate frequency range should be identified using graphs like those in Figure 9. In this case the frequency range chosen was 3 kHz to 10 MHz. Therefore, the membrane capacitance and cytoplasm conductivity (Figure 11) from 3 kHz and 10 MHz were averaged, and the resulting values are listed in Table 2.

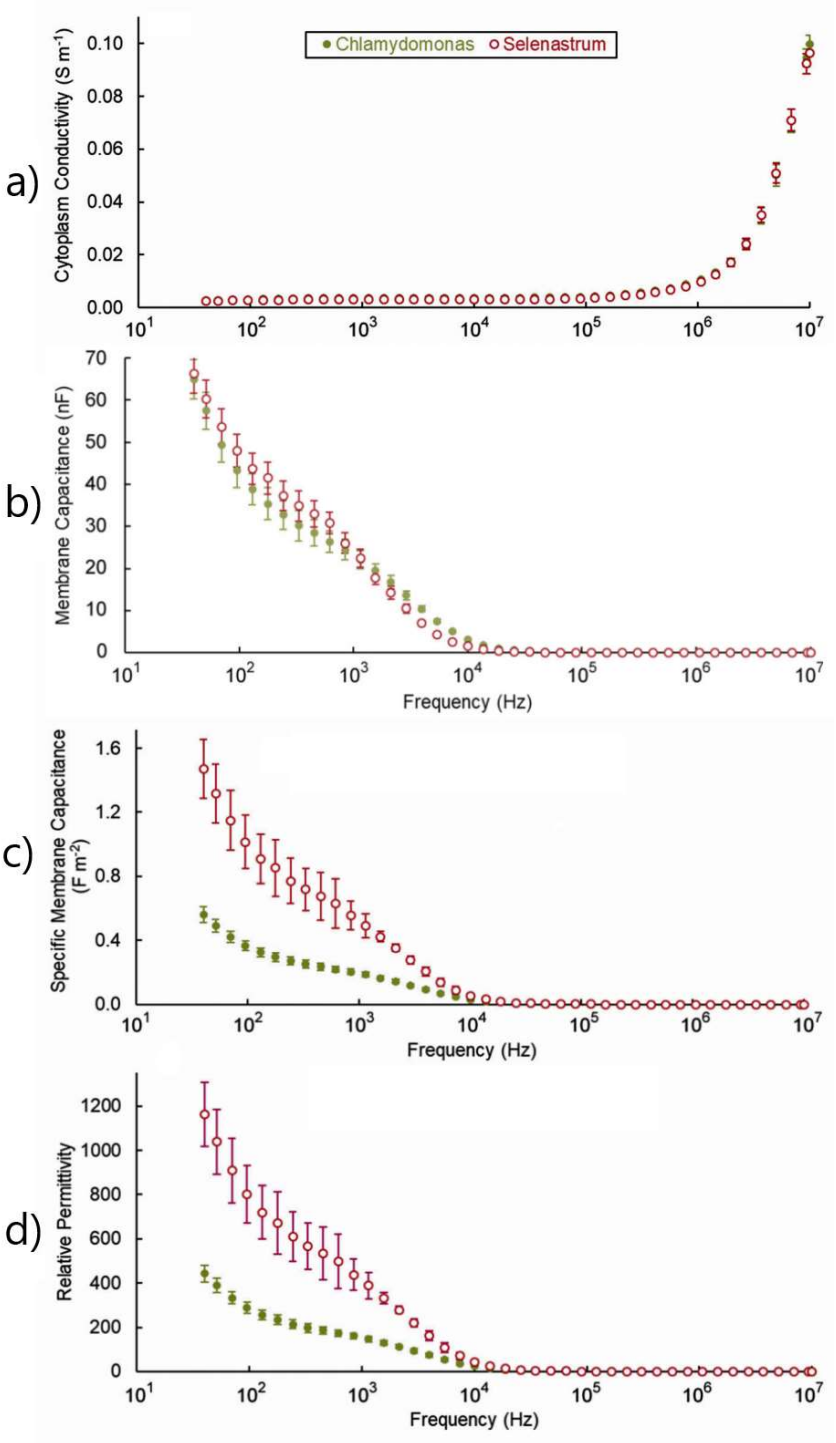

Figure 11. Average and standard deviation of a) cytoplasm conductivity, b) membrane capacitance, c) specific membrane capacitance, and d) relative permittivity for N+ C. reinhardtii and S. capricornutum.

Table 2

Measured Cytoplasm Conductivity and Membrane Capacitance Values

Specimen	Cell Diameter (μm)	Cytoplasm Conductivity (mS/m) from 3 kHz to 10 MHz	Membrane Capacitance (mF/m^2) from 3 kHz to 10 MHz
N+ Chlamydomonas reinhardtii	10-12	14.4 ± 0.9 (n = 30)	15.5 ± 3.6 (n = 30)
N- Chlamydomonas reinhardtii	10-12	14.1 ± 0.4 (n = 44)	13.2 ± 2.3 (n = 44)
Selenastrum capricornutum	5-7	14.4 ± 0.5 (n = 28)	40.6 ± 12.6 (n = 28)

On average, the cytoplasm conductivity between Selenastrum and Chlamydomonas N+ were similar, and not differentiable. However, the membrane capacitance between the two groups was different, meaning that this parameter could be used to differentiate the species. When comparing the Chlamydomonas N+ and Chlamydomonas N– test groups, there was a slight difference between the cytoplasm conductivity, and a much more prominent difference between the membrane capacitances. However, using a t-test, the difference between these means were not found to be statistically significant.

Previous studies report that the cytoplasm conductivity of healthy C. reinhardtii varies from 0.008 S/m (Siebman, Velev, & Slaveykova, 2017), to 0.2267 S/m (Hadady, Wong, Hiibel, Redelman, & Geiger, 2014), to 0.45 S/m (Michael, Hiibel, & Geiger, 2014). The variation between these results appear to originate from the different analysis methods, and different circuit models used. For example, both Michael et al. (2014) and Hadady et al. (2014) studied the effect of lipid accumulation on upper crossover frequency using dielectric spectroscopy but had vastly different results. When reading the studies, assumptions such as cytoplasm permittivity and media conductivity appear to have a notable impact on results. Additionally, one complication presented in these studies is that cell conductivity fluctuates with the cell environment, as opposed to permittivity, which is a static characteristic, so there will naturally be some variation among studies due to different media conditions. High lipid C. reinhardtii cytoplasm conductivity also ranged from .095 S/m (Hadady et al., 2014) to 0.25 S/m (Michael et al., 2014), for similar reasons mentioned above. One constant between these previous studies, however, was that there was a significant difference between the high lipid and low lipid cytoplasm conductivity, which is not present in the current results. One possible explanation for this is that differentiation based on cytoplasm conductivity of cells can only be achieved by utilizing high frequency AC generators (40-80 MHz). Complicated PCB and/or electrode setups are required to accommodate such high frequency generators and avoid interference from the surrounding environments (Petchakup et al. 2017). As a result, the curves converged as frequency approached 500 kHz, and information on the cytoplasm conductivity could not reliably be collected. There is limited impedance information available for S. capricornutum's cytoplasm conductivity

and membrane capacitance due to its small size and sickle shape, but its effective cytoplasm conductivity has been reported at 10 mS/m (Hübner, Hoettges, & Hughes, 2003).

The main strengths of this testing method were that it was fast, easy to use, and required minimum fabrication. The machine and chip used were already engineered and manufactured for general purchase. As a result, the only fabrication necessary was the chip holder, which connected the chip to the machine, and was fabricated using electrical components that were already available in the lab, making it easily reproducible in future studies. Additionally, using this method required little training. The well and sample size was such that each sample could be pipetted into the well, poured out, and the chip could be cleaned with deionized water without the use of chemicals and intricate or precise tools that may be difficult to accommodate in an in situ setting. Impedance spectroscopy also has a long experimental history dating back to the late 1800s, and has been used in a variety of fields due to its ease of use, fast processing time, and non-necessary labeling, all of which improve the quality of data and results (Sui, Foflonker, Bhattacharya, & Javanmard, 2020). Cell manipulation, long prep times, and labelling can all potentially stress the cells being studied, resulting in skewed data, changes in cell biology or behavior, and even cell death. Therefore, because this method is fast, easy to use, and doesn't require labeling, it could potentially test a wider range of phytoplankton species and more accurately characterize biologic phenomenon.

The use of cells in suspension was a source of strength and weakness. With respect to designing a lab-on-chip method for identifying phytoplankton electrical characteristics, having the cells be suspended in a well allowed for minimal training, fast

test sample preparation, and easy cleaning of each well. However, cell suspension also involves some complexities with respect to circuit modeling.

Maxwell's mixture theory, also known as the Maxwell Garnett approximation, is a theory that proposes a model for simplifying a complex electrochemical medium (Markel, 2016). At its most simplistic, this theory models spherical particles in suspension within a homogenous effective medium, under the assumption that the particles are uniformly spaced throughout the medium. The Maxwell-Garnett mixing formulas can then be used to calculate the effective permittivity of the medium and particles, as outlined in the methods section.

While there was a definitive difference in result between Chlamydomonas reinhardtii and Selenastrum capricornutum, S. capricornutum's unusual shape made it difficult to characterize, and it was thus treated as a perfect sphere wrapped in a thin membrane, and therefore the results are not considered accurate. However, there has been research that expands these formulas for use in a wider variety of complex medium conditions, such as for spheroid and elliptical particles, non-isotropic particles, non-uniformly mixed particles, and particles without membranes (Stubbe & Gimsa, 2015). While these additions are simplistic, and therefore not totally accurate, they have expanded the viability of impedance spectroscopy to accommodate a much larger range of situations. Further tests into more well-documented species may help specify further the strengths and limitations of this method by resolving some of the problems presented by S. capricornutum's shape and size. For future experiments, a comparative study using this same chip and platform could be used to characterize phytoplankton species that more closely resemble some of the alternative models derived for cells in suspension.

Another source of error was the double layer formed at the electrolyte/electrode phase boundary (Coster et al., 1996). As mentioned above, an AC current at low frequencies will establish ionic concentrations and gradients which will be different for positive and negative ions. This in turn will yield diffusion currents that are out of phase with the AC electrical current, resulting in impedances with characteristics of very large capacitors. As the frequency increases, the time for the establishment of the AC ionic concentrations and diffusions diminishes, causing the impedance reactive component to decrease as well. However, at a phase boundary, such as the one formed between an electrode and electrolyte solution, this is not necessarily the case. As charges diffuse into the solution, it causes a surface with a net charge, and this surface charge then causes an electric field which attracts ions from within the solution. As these ions are absorbed, they form a diffuse layer across the surface (Figure 12). This diffuse layer of ions and the layer of charges at the surface form a double layer. As a result, the interface of electrodes and electrolyte solutions, in turn, can exhibit dispersions at frequencies that are like those of membrane systems, resulting in similar impedance charts. This phenomenon is shown in Figure 9. The impedance formed at these interfaces must be eliminated for an accurate impedance reading of the system. It is theoretically possible to measure the interfacial impedance separately, and then subtract that figure from the system impedance, but doing so requires very high accuracy for both the electrode and electrode-system to avoid instrumental error. As a result, such estimates are generally considered unreliable.

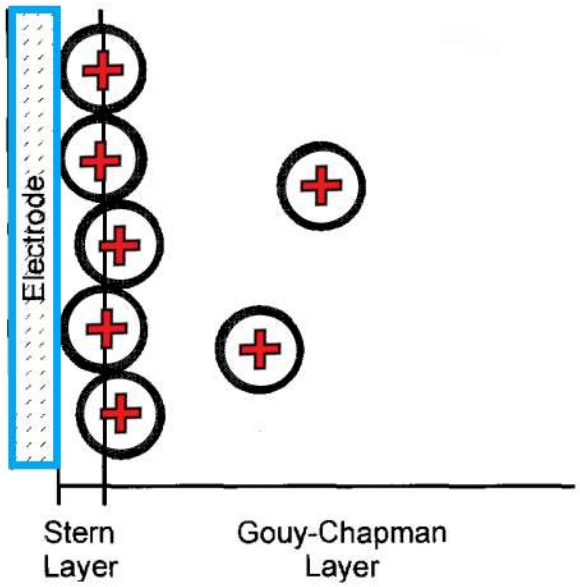

Figure 12. Double layer formed from the electrode's net charge and a layer of diffuse ions. Modified from Coster et al. (1996).

One possible way to improve results is to experiment with different electrode sizes and configurations. As previously mentioned, electrolyte/electrode layer impedance skews impedance results, and is difficult to measure and adjust for. However, previous research has established that increasing electrode size decreases the electrode/electrolyte layer impedance, because of the inverse relationship between the radius of the electrode and the faradic impedance (Zhang et al., 2017). Additionally, electrode size has a more significant effect on impedance measurements at lower frequencies, because as the frequency increases, the electrode has less time to establish a charged surface, which causes the electrode/electrolyte layer to have less of an impact, until, at sufficiently high frequency, the resistance of the conductive medium is the only thing being sensed. As electrode size decreased, impedance magnitude and phase shifted to the right, meaning that higher frequencies were required to achieve the same results as larger electrodes. Similar results were also found in experiments using confluent cell monolayers, which

normalized the impedance and resistance of the cell covered electrodes by comparing it to the impedance and resistance of the electrolyte medium (Lai, Chu, Lo, Hung, & Lo, 2019). This allowed the researchers to identify at which frequencies the confluent layer impedance varied most from the electrolyte impedance and led them to conclude that as electrode size decreases, the frequency at which the electrode is most sensitive to impedance changes increases. Additionally, while microfluidics minimize sample size, and thus reduce sample preparation time, they can still require extensive preparation (centrifugation, dilution, encapsulation, etc.), which limits in situ viability. Microfluidic chips have great potential for minimizing the space and resources needed for in situ experiments, so understanding how electrode size and configuration affects results, and how to optimize sensitivity while minimizing space requirement is vital to future research.

Along with diversifying the phytoplankton species and experimenting with electrode size and configuration, different stressors could also be utilized (Häder & Gao, 2015). Nitrogen deprivation was chosen for this experiment because past research suggested that it would cause C. reinhardtii to produce lipids, theoretically changing the electrical characteristics in a predictable way. However, species react differently to different environmental changes such as nutrient availability, increased UV radiation, ocean acidification, and the presence of pollutants. Certain environmental changes may cause one species to decline, but not affect the population of another, or may even cause population growth. For example, diatoms have been shown to take up and store nitrate more efficiently than other phytoplankton species, which could cause them to yield

different experimental results than Chlamydomonas under the same conditions (Lampe, Wang, Cassar, & Marchetti, 2019).

Microfluidic impedance spectroscopy has potential with respect to ease of use and size requirements, but requires further investigation into what circumstances it is viable to use in. These circumstances will be defined as a larger variety of phytoplankton, stressors, and equipment are researched. While this study demonstrated that this platform could characterize the electrical characteristics of different species and cells grown in different nitrogen conditions, it did not explore if this characterization was sufficient for differentiation between samples. Future research could explore this by using this system to identify random samples with distinct electrical characteristics and recording how many samples can be correctly identified using the impedance spectroscopy data and results.

CHAPTER IV

CONCLUSION

Impedance spectroscopy has been used in a variety of industrial and research applications, and when combined with microfluidic technology, has the potential to be used for in situ phytoplankton characterization. In this experiment, the healthy Chlamydomonas reinhardtii and Selenastrum capricornutum samples had indistinguishable cytoplasm conductivity but were differentiable by their membrane capacitance. There were slight differences between the electrical characteristics of the stressed and unstressed C. reinhardtii. These results are promising but limited by computational problems related to Maxwell's mixture theory, and electrode/electrolyte double layer impedances. Further investigation into instrumentation, phytoplankton species, and stressors are needed to understand the capabilities of this system.

REFERENCES

Aberg, P., Nicander, I., Hansson, J., Geladi, P., Holmgren, U., & Ollmar, S. (2004). Skin cancer identification using multifrequency electrical impedance-a potential screening tool. *IEEE Transactions on Biomedical Engineering, 51*(12), 2097-2102.

Asami, K., & Yonezawa, T. (1995). Dielectric behavior of non-spherical cells in culture. *Biochimica et Biophysica Acta (BBA) - General Subjects, 1245*(3), 317-324. doi:https://doi.org/10.1016/0304-4165(95)00116-6

Basiji, D. A., Ortyn, W. E., Liang, L., Venkatachalam, V., & Morissey, P. (2007). Cellular Image Analysis and Imaging by Flow Cytometry. *Clinics in Laboratory Medicine, 27*(3), 653-670. doi:10.1016/j.cll.2007.05.008

Behrenfeld, M. J., O'Malley, R. T., Siegel, D. A., McClain, C. R., Sarmiento, J. L., Feldman, G. C., . . . Boss, E. S. (2006). Climate-driven trends in contemporary ocean productivity. *Nature, 444*(7120), 752-755.

Benazzi, G., Holmes, D., Sun, T., Mowlem, M. C., & Morgan, H. (2007). Discrimination and analysis of phytoplankton using a microfluidic cytometer. *IET nanobiotechnology, 1*(6), 94-101.

Bopp, L., Aumont, O., Cadule, P., Alvain, S., & Gehlen, M. (2005). Response of diatoms distribution to global warming and potential implications: A global model study. *Geophysical Research Letters, 32*(19). doi:10.1029/2005GL023653

Borowitzka, M. (1997). Microalgae for aquaculture: Opportunities and constraints. *Journal of Applied Phycology, 9*(5), 393-401.

Brown, B. H., Milnes, P., Abdul, S., & Tidy, J. A. (2005). Detection of cervical intraepithelial neoplasia using impedance spectroscopy: a prospective study. *BJOG: An International Journal of Obstetrics & Gynaecology, 112*(6), 802-806. doi:10.1111/j.1471-0528.2004.00530.x

Changjun, X., & Shuhai, Q. (2011). Drawing impedance spectroscopy for Fuel Cell by EIS. *Procedia Environmental Sciences, 11*, 589-596. doi:https://doi.org/10.1016/j.proenv.2011.12.092

Coster, H. G. L., Chilcott, T. C., & Coster, A. C. F. (1996). Impedance spectroscopy of interfaces, membranes and ultrastructures. *Bioelectrochemistry and Bioenergetics, 40*(2), 79-98. doi:https://doi.org/10.1016/0302-4598(96)05064-7

Cummings, B. S., Wills, L. P., & Schnellmann, R. G. (2012). Measurement of Cell Death in Mammalian Cells. *Current Protocols in Pharmacology, 56*(1), 12.18.11-12.18.24. doi:10.1002/0471141755.ph1208s56

Das, D., Kamil, F. A., Biswas, K., & Das, S. (2014). Evaluation of single cell electrical parameters from bioimpedance of a cell suspension. *RSC Advances, 4*(35), 18178-18185. doi:10.1039/C4RA00400K

De Ninno, A., Reale, R., Giovinazzo, A., Bertani, F. R., Businaro, L., Bisegna, P., . . . Caselli, F. (2020). High-throughput label-free characterization of viable, necrotic and apoptotic human lymphoma cells in a coplanar-electrode microfluidic

impedance chip. *Biosensors and Bioelectronics, 150*, 111887. doi:https://doi.org/10.1016/j.bios.2019.111887
Diaz, R. J., & Rosenberg, R. (2008). Spreading Dead Zones and Consequences for Marine Ecosystems. *Science, 321*(5891), 926-929.
Dismukes, G. C., Carrieri, D., Bennette, N., Ananyev, G. M., & Posewitz, M. C. (2008). Aquatic phototrophs: efficient alternatives to land-based crops for biofuels. *Current Opinion in Biotechnology, 19*(3), 235-240. doi:https://doi.org/10.1016/j.copbio.2008.05.007
Foster, K., & Schwan, H. (1989). Dielectric properties of tissues and biological materials: A critical review, CRC Biomed. *Eng, 17*, 25-104.
Galluzzi, L., Vitale, I., Aaronson, S. A., Abrams, J. M., Adam, D., Agostinis, P., . . . Kroemer, G. (2018). Molecular mechanisms of cell death: recommendations of the Nomenclature Committee on Cell Death 2018. *Cell Death & Differentiation, 25*(3), 486-541. doi:10.1038/s41418-017-0012-4
Georgianna, D. R., & Mayfield, S. P. (2012). Exploiting diversity and synthetic biology for the production of algal biofuels. *Nature, 488*, 329-335. doi:https://doi.org/10.1038/nature11479
Girault, M., Beneyton, T., Amo, Y. d., & Baret, J.-C. (2018). Microfluidic technology for plankton research. *Current Opinion in Biotechnology, 55*, 134-150. doi:https://doi.org/10.1016/j.copbio.2018.09.010
Girault, M., Beneyton, T., del Amo, Y., & Baret, J.-C. (2019). Microfluidic technology for plankton research. *Current Opinion in Biotechnology, 55*, 134-150. doi:https://doi.org/10.1016/j.copbio.2018.09.010
Goda, K., Ayazi, A., Gossett, D. R., Sadasivam, J., Lonappan, C. K., Sollier, E., . . . Jalali, B. (2012). High-throughput single-microparticle imaging flow analyzer. *Proceedings of the National Academy of Sciences, 109*(29), 11630-11635. doi:https://doi.org/10.1073/pnas.1204718109
Godhe, A., Anderson, D., & Rehnstam-Holm, A.-S. (2002). PCR amplification of microalgal DNA for sequencing and species identification: Studies on fixatives and algal growth stages. *Harmful Algae, 1*, 375-382. doi:10.1016/S1568-9883(02)00049-5
Hadady, H., Wong, J. J., Hiibel, S. R., Redelman, D., & Geiger, E. J. (2014). High frequency dielectrophoretic response of microalgae over time. *Electrophoresis, 35*(24), 3533-3540. doi:10.1002/elps.201400306
Häder, D.-P., & Gao, K. (2015). Interactions of anthropogenic stress factors on marine phytoplankton. *Frontiers in Environmental Science, 3*(14). doi:10.3389/fenvs.2015.00014
Hallegraeff, G. M. (2010). OCEAN CLIMATE CHANGE, PHYTOPLANKTON COMMUNITY RESPONSES, AND HARMFUL ALGAL BLOOMS: A FORMIDABLE PREDICTIVE CHALLENGE. *Journal of Phycology, 46*(2), 220-235. doi:10.1111/j.1529-8817.2010.00815.x
Halter Ryan, J., Schned, A., Heaney, J., Hartov, A., Schutz, S., & Paulsen Keith, D. (2008). Electrical Impedance Spectroscopy of Benign and Malignant Prostatic Tissues. *Journal of Urology, 179*(4), 1580-1586. doi:10.1016/j.juro.2007.11.043
Harris, E. H. (2001). CHLAMYDOMONAS AS A MODEL ORGANISM. *Annu Rev Plant Physiol Plant Mol Biol, 52*, 363-406. doi:10.1146/annurev.arplant.52.1.363

Hashemi, N., Erickson, J. S., Golden, J. P., Jackson, K. M., & Ligler, F. S. (2011). Microflow Cytometer for optical analysis of phytoplankton. *Biosensors and Bioelectronics, 26*(11), 4263-4269. doi:https://doi.org/10.1016/j.bios.2011.03.042

Hillary, S. L., Brown, B. H., Brown, N. J., & Balasubramanian, S. P. (2020). Use of Electrical Impedance Spectroscopy for Intraoperative Tissue Differentiation During Thyroid and Parathyroid Surgery. *World J Surg, 44*(2), 479-485. doi:10.1007/s00268-019-05169-7

Hübner, Y., Hoettges, K. F., & Hughes, M. P. (2003). Water quality test based on dielectrophoretic measurements of fresh water algae Selenastrum capricornutum. *Journal of Environmental Monitoring, 5*(6), 861-864. doi:10.1039/B309131G

Hughes, M. A., Allen, J. A., & Donne, S. W. (2020). Characterization of carbonate derived carbons through electrochemical impedance spectroscopy. *Electrochimica Acta, 338*. doi:10.1016/j.electacta.2020.135847

Ivanova, I., & Groudeva, V. (2006). Use of Selenastrum Capricornutum Growth Inhibition Test for Testing Toxicity of Metal Ions in Soil and Water. *Biotechnology & Biotechnological Equipment, 20*(1), 179-183. doi:https://doi.org/10.1080/13102818.2006.10817329

Janicka, E., Mielniczek, M., Gawel, L., Darowicki, K., & Landowska, P. (2020). The impact of air humidity on the operation of proton exchange membrane fuel cells determined using dynamic electrochemical

impedance spectroscopy. *Electrochimica Acta, 341*. doi:https://doi.org/10.1016/j.electacta.2020.136036

Keshtkar, A., Salehnia, Z., Keshtkar, A., & Shokouhi, B. (2012). Bladder cancer detection using electrical impedance technique (Tabriz Mark 1). *Pathology research international, 2012*.

Kuntanawat, P., Ruenin, J., Phatthanakun, R., Kunhorm, P., Surareungchai, W., Sukprasong, S., & Chomnawang, N. (2014). An electrostatic microwell-based biochip for phytoplanktonic cell trapping. *Biomicrofluidics, 8*(3), 034108. doi:10.1063/1.4882196

Lai, Y.-T., Chu, Y.-S., Lo, J.-C., Hung, Y.-H., & Lo, C.-M. (2019). Effects of electrode diameter on the detection sensitivity and frequency characteristics of electric cell-substrate impedance sensing. *Sensors & Actuators: B. Chemical, 288*, 707-715. doi:10.1016/j.snb.2019.02.098

Lampe, R. H., Wang, S., Cassar, N., & Marchetti, A. (2019). Strategies among phytoplankton in response to alleviation of nutrient stress in a subtropical gyre. *The ISME Journal, 13*(12), 2984-2997. doi:10.1038/s41396-019-0489-6

Lasia, A. (2014). *Electrochemical impedance spectroscopy and its applications* (1 ed.): Springer-Verlag New York.

Lindsey, R., & Scott, M. (2010). What are Phytoplankton? Retrieved from https://earthobservatory.nasa.gov/features/Phytoplankton

Markel, V. A. (2016). Introduction to the Maxwell Garnett approximation: tutorial. *Journal of the Optical Society of America A, 33*(7), 1244-1256. doi:10.1364/JOSAA.33.001244

Mata, T. M., Martins, A. A., & Caetano, N. S. (2010). Microalgae for biodiesel production and other applications: A review. *Renewable and Sustainable Energy Reviews, 14*(1), 217-232. doi:https://doi.org/10.1016/j.rser.2009.07.020

Maw, M. M., Pan, X., Peng, Z., Wang, Y., Zhao, L., Dai, B., & Wang, J. (2018). A Changeable Lab-on-a-Chip Detector for Marine Nonindigenous Microorganisms in Ship's Ballast Water. *Micromachines (Basel), 9*(1). doi:10.3390/mi9010020

Maxwell, J. C. (1954). *A Treatise on Electricity and Magnetism* (2 ed. Vol. 2): Dover Publications Inc.

Meng, J., Yanga, Z., Chen, L., Zeng, X., Hongzhe Chen, F. C., & Jiangab, Y. (2020). The investigation on the electrochemical performance of CuI as cathode material for zinc storage. *Electrochimica Acta, 338*. doi:https://doi.org/10.1016/j.electacta.2020.135915

Michael, K. A., Hiibel, S. R., & Geiger, E. J. (2014). Dependence of the dielectrophoretic upper crossover frequency on the lipid content of microalgal cells. *Algal Research, 6*, 17-21. doi:https://doi.org/10.1016/j.algal.2014.08.004

Morgan, H., Holmes, D., & Green, N. G. (2006). High speed simultaneous single particle impedance and fluorescence analysis on a chip. *Current Applied Physics, 6*(3), 367-370. doi:10.1016/j.cap.2005.11.020

Morgan, H., Sun, T., Holmes, D., Gawad, S., & Green, N. G. (2006). Single cell dielectric spectroscopy. *Journal of Physics D: Applied Physics, 40*(1), 61.

Murdoch, C., Brown, B. H., Hearnden, V., Speight, P. M., D'Apice, K., Hegarty, A. M., . . . Thornhill, M. H. (2014). Use of electrical impedance spectroscopy to detect malignant and potentially malignant oral lesions. *International journal of nanomedicine, 9*, 4521-4532. doi:10.2147/IJN.S64087

Mutanda, T., Ramesh, D., Karthikeyan, S., Kumari, S., Anandraj, A., & Buxa, F. (2011). Bioprospecting for hyper-lipid producing microalgal strains for sustainable biofuel production. *Bioresource Technology, 102*(1), 57-70. doi:https://doi.org/10.1016/j.biortech.2010.06.077

Nejad, S., Gladwin, D. T., & Stone, D. A. (2016). A systematic review of lumped-parameter equivalent circuit models for real-time estimation of lithium-ion battery states. *Journal of Power Sources, 316*, 183-196. doi:10.1016/j.jpowsour.2016.03.042

Newsted, J. L. (2004). Effect of light, temperature, and pH on the accumulation of phenol by Selenastrum capricornutum, a green alga. *Ecotoxicology and Environmental Safety, 59*, 237-243. doi:10.1016/j.ecoenv.2003.07.009

Richardson, A. J., & Schoeman, D. S. (2004). Climate Impact on Plankton Ecosystems in the Northeast Atlantic. *Science, 305*(5690), 1609. doi:10.1126/science.1100958

Rollo, E., Tenaglia, E., Genolet, R., Bianchi, E., Harari, A., Coukos, G., & Guiducci, C. (2017). Label-free identification of activated T lymphocytes through tridimensional microsensors on chip. *Biosensors and Bioelectronics, 94*, 193-199. doi:https://doi.org/10.1016/j.bios.2017.02.047

Sabuncu, A. C., Zhuang, J., Kolb, J. F., & Beskok, A. (2012). Microfluidic impedance spectroscopy as a tool for quantitative biology and biotechnology.

Sasso, S., Stibor, H., Mittag, M., & Grossman, A. R. (2018). The Natural History of Model Organisms: From molecular manipulation of domesticated Chlamydomonas reinhardtii to survival in nature. *eLife*. doi:10.7554/eLife.39233

Schonbrun, E., Gorthi, S. S., & Schaak, D. (2012). Microfabricated multiple field of view imaging flow cytometry. *Lab on a Chip, 12*(2), 268-273.

Searchinger, T., Heimlich, R., Houghton, R. A., Dong, F., Elobeid, A., Fabiosa, J., . . . Yu, T.-H. (2008). Use of U.S. Croplands for Biofuels Increases Greenhouse Gases Through Emissions from Land-Use Change. *Science, 319*(5867), 1238-1240. doi:10.1126/science.1151861

Siebman, C., Velev, O. D., & Slaveykova, V. I. (2017). Alternating current-dielectrophoresis collection and chaining of phytoplankton on chip: comparison of individual species and artificial communities. *Biosensors, 7*(4). doi:10.3390/bios7010004

Stojadinovic, A., Nissan, A., Shriver, C. D., Mittendorf, E. A., Akin, M. D., Dickerson, V., . . . Gur, D. (2008). Electrical impedance scanning as a new breast cancer risk stratification tool for young women. *Journal of Surgical Oncology, 97*(2), 112-120. doi:10.1002/jso.20931

Stubbe, M., & Gimsa, J. (2015). Maxwell's Mixing Equation Revisited: Characteristic Impedance Equations for Ellipsoidal Cells. *Biophysical Journal, 109*(2), 194-208. doi:https://doi.org/10.1016/j.bpj.2015.06.021

Sui, J., Foflonker, F., Bhattacharya, D., & Javanmard, M. (2020). Electrical impedance as an indicator of microalgal cell health. *Scientific Reports, 10*(1), 1251. doi:10.1038/s41598-020-57541-6

Sun, T., & Morgan, H. (2010). Single-cell microfluidic impedance cytometry: a review. *Microfluidics and Nanofluidics, 8*(4), 423-443. doi:10.1007/s10404-010-0580-9

Tang, J., Yin, W., & Lu, M. (2020). Bio-impedance spectroscopy for frozen-thaw of bio-samples: Non-contact inductive measurement and finite element (FE) based cell modelling. *Journal of Food Engineering, 272*, 109784. doi:https://doi.org/10.1016/j.jfoodeng.2019.109784

Tidy, J., Brown, B., Healey, T., Daayana, S., Martin, M., Prendiville, W., & Kitchener, H. (2013). Accuracy of detection of high-grade cervical intraepithelial neoplasia using electrical impedance spectroscopy with colposcopy. *BJOG: An International Journal of Obstetrics & Gynaecology, 120*(4), 400-411. doi:10.1111/1471-0528.12096

Wang, B., Li, Y., Wu, N., & Lan, C. Q. (2008). CO2 bio-mitigation using microalgae. *Applied Microbiology and Biotechnology, 79*(5), 707-718. doi:10.1007/s00253-008-1518-y

Wang, J., Zhao, J., Wang, Y., Wang, W., Gao, Y., Xu, R., & Zhao, W. (2016). A New Microfluidic Device for Classification of Microalgae Cells Based on Simultaneous Analysis of Chlorophyll Fluorescence, Side Light Scattering, Resistance Pulse Sensing. *Micromachines (Basel), 7*(11). doi:10.3390/mi7110198

Yamagishi, T., Yamaguchi, H., Suzuki, S., Horie, Y., & Tatarazako, N. (2017). Cell reproductive patterns in the green alga Pseudokirchneriella subcapitata (=Selenastrum capricornutum) and their variations under exposure to the typical toxicants potassium dichromate and 3,5-DCP. *Plos One*. doi:https://doi.org/10.1371/journal.pone.0171259

Yang, L., Chen, J., Qin, S., Zeng, M., Jiang, Y., Hu, L., . . . Wang, J. (2018). Growth and lipid accumulation by different nutrients in the microalga Chlamydomonas reinhardtii. *Biotechnology for Biofuels volume 11*. doi:https://doi.org/10.1186/s13068-018-1041-z

Zabara, M. A., & Ulgut, B. (2020). Electrochemical Impedance Spectroscopy based voltage modeling of lithium Thionyl Chloride (Li\SOCl2) primary battery at arbitrary discharge. *Electrochimica Acta, 334*. doi:https://doi.org/10.1016/j.electacta.2019.135584

Zhang, X., Wang, W., Nordin, A. N., Li, F., Jang, S., & Voiculescu, I. (2017). The influence of the electrode dimension on the detection sensitivity of electric cell–substrate impedance sensing (ECIS) and its mathematical modeling. *Sensors and Actuators B: Chemical, 247*, 780-790. doi:https://doi.org/10.1016/j.snb.2017.03.047

Zhu, L. (2015). Biorefinery as a promising approach to promote microalgae industry: An innovative framework. *Renewable and Sustainable Energy Reviews, 41*, 1376-1384. doi:https://doi.org/10.1016/j.rser.2014.09.040

Zhu, W. H., Zhu, Y., & Tatarchuk, B. J. (2011). A simplified equivalent circuit model for simulation of Pb–acid batteries at load for energy storage application. *Energy Conversion and Management, 52*(8-9), 2794-2799. doi:https://doi.org/10.1016/j.enconman.2011.02.013

APPENDIX A
CHA1H4 DATA EXAMPLE

4294A REV1.11
"DATE: 9 -100"

"MEASURE PARAMETER: IMPEDANCE MAG PHASE (DEG)"
"ADAPTER: PROBE"
"SWEEP TYPE: LOG FREQ"
"NUMBER of POINTS: 201"
"POINT DELAY TIME: 0 Sec"
"SWEEP DELAY TIME: 0 Sec"
"OSC LEVEL: 10 mVolt"
"DC BIAS: OFF"
"BW: 3"
"SWEEP AVERAGING: OFF"
"POINT AVERAGING: OFF"

"TRACE: A"
"FORMAT: LINEAR"

"Frequency"	"Data Trace Real"	"Data Trace Imag"
4.00000000000e+01	2.723419e+05	0.000000e+00
4.25650000000e+01	2.620703e+05	0.000000e+00
4.52940000000e+01	2.478301e+05	0.000000e+00
4.81980000000e+01	2.392117e+05	0.000000e+00
5.12880000000e+01	2.299455e+05	0.000000e+00
5.45770000000e+01	2.210589e+05	0.000000e+00
5.80760000000e+01	2.119838e+05	0.000000e+00
6.18000000000e+01	2.012848e+05	0.000000e+00
6.57620000000e+01	1.939943e+05	0.000000e+00
6.99790000000e+01	1.859008e+05	0.000000e+00
7.44660000000e+01	1.799163e+05	0.000000e+00
7.92400000000e+01	1.711966e+05	0.000000e+00
8.43210000000e+01	1.665187e+05	0.000000e+00
8.97280000000e+01	1.618885e+05	0.000000e+00
9.54810000000e+01	1.549971e+05	0.000000e+00
1.01603000000e+02	1.511871e+05	0.000000e+00
1.08117000000e+02	1.464282e+05	0.000000e+00
1.15050000000e+02	1.414110e+05	0.000000e+00
1.22426000000e+02	1.377716e+05	0.000000e+00
1.30276000000e+02	1.336946e+05	0.000000e+00
1.38629000000e+02	1.298807e+05	0.000000e+00
1.47518000000e+02	1.274685e+05	0.000000e+00

1.56976000000e+02	1.233159e+05	0.000000e+00
1.67041000000e+02	1.215028e+05	0.000000e+00
1.77751000000e+02	1.182420e+05	0.000000e+00
1.89148000000e+02	1.159087e+05	0.000000e+00
2.01276000000e+02	1.139334e+05	0.000000e+00
2.14181000000e+02	1.124758e+05	0.000000e+00
2.27914000000e+02	1.094298e+05	0.000000e+00
2.42528000000e+02	1.086098e+05	0.000000e+00
2.58078000000e+02	1.063083e+05	0.000000e+00
2.74625000000e+02	1.057445e+05	0.000000e+00
2.92234000000e+02	1.044986e+05	0.000000e+00
3.10971000000e+02	1.024442e+05	0.000000e+00
3.30910000000e+02	1.016862e+05	0.000000e+00
3.52127000000e+02	1.001189e+05	0.000000e+00
3.74705000000e+02	1.010029e+05	0.000000e+00
3.98730000000e+02	9.897088e+04	0.000000e+00
4.24296000000e+02	9.763075e+04	0.000000e+00
4.51501000000e+02	9.627216e+04	0.000000e+00
4.80450000000e+02	9.660912e+04	0.000000e+00
5.11255000000e+02	9.557505e+04	0.000000e+00
5.44036000000e+02	9.578354e+04	0.000000e+00
5.78918000000e+02	9.453533e+04	0.000000e+00
6.16037000000e+02	9.473710e+04	0.000000e+00
6.55536000000e+02	9.393191e+04	0.000000e+00
6.97567000000e+02	9.350216e+04	0.000000e+00
7.42294000000e+02	9.303916e+04	0.000000e+00
7.89888000000e+02	9.253562e+04	0.000000e+00
8.40534000000e+02	9.178591e+04	0.000000e+00
8.94427000000e+02	9.236825e+04	0.000000e+00
9.51776000000e+02	9.147392e+04	0.000000e+00
1.01280200000e+03	9.132016e+04	0.000000e+00
1.07774000000e+03	9.123580e+04	0.000000e+00
1.14684300000e+03	9.053888e+04	0.000000e+00
1.22037600000e+03	9.057451e+04	0.000000e+00
1.29862300000e+03	9.046017e+04	0.000000e+00
1.38188800000e+03	9.033738e+04	0.000000e+00
1.47049200000e+03	8.955661e+04	0.000000e+00
1.56477600000e+03	8.958538e+04	0.000000e+00
1.66510600000e+03	8.958043e+04	0.000000e+00
1.77186900000e+03	8.931942e+04	0.000000e+00
1.88547800000e+03	8.877437e+04	0.000000e+00
2.00637000000e+03	8.915211e+04	0.000000e+00
2.13501400000e+03	8.879768e+04	0.000000e+00
2.27190700000e+03	8.869114e+04	0.000000e+00
2.41757600000e+03	8.833037e+04	0.000000e+00
2.57258600000e+03	8.868421e+04	0.000000e+00

2.73753400000e+03	8.826478e+04	0.000000e+00
2.91305900000e+03	8.799566e+04	0.000000e+00
3.09983800000e+03	8.792168e+04	0.000000e+00
3.29859300000e+03	8.779517e+04	0.000000e+00
3.51009100000e+03	8.783241e+04	0.000000e+00
3.73515000000e+03	8.794666e+04	0.000000e+00
3.97464000000e+03	8.760468e+04	0.000000e+00
4.22948500000e+03	8.752834e+04	0.000000e+00
4.50067000000e+03	8.714745e+04	0.000000e+00
4.78924300000e+03	8.748836e+04	0.000000e+00
5.09631900000e+03	8.672903e+04	0.000000e+00
5.42308400000e+03	8.715053e+04	0.000000e+00
5.77080000000e+03	8.730781e+04	0.000000e+00
6.14081000000e+03	8.702698e+04	0.000000e+00
6.53454600000e+03	8.698265e+04	0.000000e+00
6.95352600000e+03	8.657091e+04	0.000000e+00
7.39937100000e+03	8.655970e+04	0.000000e+00
7.87380200000e+03	8.646514e+04	0.000000e+00
8.37865300000e+03	8.659975e+04	0.000000e+00
8.91587300000e+03	8.621208e+04	0.000000e+00
9.48753900000e+03	8.633109e+04	0.000000e+00
1.00958590000e+04	8.645130e+04	0.000000e+00
1.07431840000e+04	8.623693e+04	0.000000e+00
1.14320130000e+04	8.611628e+04	0.000000e+00
1.21650080000e+04	8.593238e+04	0.000000e+00
1.29450010000e+04	8.574572e+04	0.000000e+00
1.37750060000e+04	8.581748e+04	0.000000e+00
1.46582290000e+04	8.549942e+04	0.000000e+00
1.55980820000e+04	8.535892e+04	0.000000e+00
1.65981960000e+04	8.526105e+04	0.000000e+00
1.76624360000e+04	8.505741e+04	0.000000e+00
1.87949120000e+04	8.479454e+04	0.000000e+00
2.00000000000e+04	8.476204e+04	0.000000e+00
2.12823560000e+04	8.453448e+04	0.000000e+00
2.26469330000e+04	8.424202e+04	0.000000e+00
2.40990040000e+04	8.379409e+04	0.000000e+00
2.56441790000e+04	8.358777e+04	0.000000e+00
2.72884270000e+04	8.343970e+04	0.000000e+00
2.90381000000e+04	8.300466e+04	0.000000e+00
3.08999580000e+04	8.257637e+04	0.000000e+00
3.28811950000e+04	8.215980e+04	0.000000e+00
3.49894650000e+04	8.189850e+04	0.000000e+00
3.72329110000e+04	8.132441e+04	0.000000e+00
3.96202030000e+04	8.084809e+04	0.000000e+00
4.21605620000e+04	8.027759e+04	0.000000e+00
4.48638040000e+04	8.036788e+04	0.000000e+00

4.77403720000e+04	7.962717e+04	0.000000e+00
5.08013780000e+04	7.869729e+04	0.000000e+00
5.40586500000e+04	7.791980e+04	0.000000e+00
5.75247710000e+04	7.723212e+04	0.000000e+00
6.12131310000e+04	7.613030e+04	0.000000e+00
6.51379810000e+04	7.536301e+04	0.000000e+00
6.93144840000e+04	7.439516e+04	0.000000e+00
7.37587750000e+04	7.241999e+04	0.000000e+00
7.84880240000e+04	7.150072e+04	0.000000e+00
8.35205020000e+04	6.957579e+04	0.000000e+00
8.88756510000e+04	6.843665e+04	0.000000e+00
9.45741610000e+04	6.723485e+04	0.000000e+00
1.00638046000e+05	6.625955e+04	0.000000e+00
1.07090734000e+05	6.566719e+04	0.000000e+00
1.13957155000e+05	6.336929e+04	0.000000e+00
1.21263834000e+05	6.103245e+04	0.000000e+00
1.29039002000e+05	5.954810e+04	0.000000e+00
1.37312697000e+05	5.817225e+04	0.000000e+00
1.46116882000e+05	5.592221e+04	0.000000e+00
1.55485573000e+05	5.416256e+04	0.000000e+00
1.65454962000e+05	5.271716e+04	0.000000e+00
1.76063567000e+05	5.070758e+04	0.000000e+00
1.87352373000e+05	4.900879e+04	0.000000e+00
1.99364991000e+05	4.620659e+04	0.000000e+00
2.12147832000e+05	4.375938e+04	0.000000e+00
2.25750280000e+05	4.184400e+04	0.000000e+00
2.40224887000e+05	3.994274e+04	0.000000e+00
2.55627573000e+05	3.791928e+04	0.000000e+00
2.72017846000e+05	3.603916e+04	0.000000e+00
2.89459027000e+05	3.446809e+04	0.000000e+00
3.08018497000e+05	3.283134e+04	0.000000e+00
3.27767960000e+05	3.091577e+04	0.000000e+00
3.48783714000e+05	2.936745e+04	0.000000e+00
3.71146951000e+05	2.772343e+04	0.000000e+00
3.94944070000e+05	2.604278e+04	0.000000e+00
4.20267008000e+05	2.462238e+04	0.000000e+00
4.47213595000e+05	2.335775e+04	0.000000e+00
4.75887939000e+05	2.189141e+04	0.000000e+00
5.06400817000e+05	2.082797e+04	0.000000e+00
5.38870114000e+05	1.959583e+04	0.000000e+00
5.73421270000e+05	1.857899e+04	0.000000e+00
6.10187769000e+05	1.751629e+04	0.000000e+00
6.49311654000e+05	1.642527e+04	0.000000e+00
6.90944077000e+05	1.550600e+04	0.000000e+00
7.35245878000e+05	1.457529e+04	0.000000e+00
7.82388212000e+05	1.368439e+04	0.000000e+00

8.32553207000e+05	1.290367e+04	0.000000e+00
8.85934671000e+05	1.216699e+04	0.000000e+00
9.42738836000e+05	1.144065e+04	0.000000e+00
1.00318515800e+06	1.075232e+04	0.000000e+00
1.06750716400e+06	1.012278e+04	0.000000e+00
1.13595335500e+06	9.541871e+03	0.000000e+00
1.20878816300e+06	8.981103e+03	0.000000e+00
1.28629297700e+06	8.420781e+03	0.000000e+00
1.36876722800e+06	7.907718e+03	0.000000e+00
1.45652954500e+06	7.482873e+03	0.000000e+00
1.54991898800e+06	6.995220e+03	0.000000e+00
1.64929635300e+06	6.582506e+03	0.000000e+00
1.75504557500e+06	6.185963e+03	0.000000e+00
1.86757520300e+06	5.811442e+03	0.000000e+00
1.98731998000e+06	5.468221e+03	0.000000e+00
2.11474252700e+06	5.141804e+03	0.000000e+00
2.25033512500e+06	4.837982e+03	0.000000e+00
2.39462161900e+06	4.548956e+03	0.000000e+00
2.54815944300e+06	4.276324e+03	0.000000e+00
2.71154177100e+06	4.017387e+03	0.000000e+00
2.88539981200e+06	3.775966e+03	0.000000e+00
3.07040524400e+06	3.550192e+03	0.000000e+00
3.26727281500e+06	3.335936e+03	0.000000e+00
3.47676309700e+06	3.142870e+03	0.000000e+00
3.69968543000e+06	2.948716e+03	0.000000e+00
3.93690105000e+06	2.771883e+03	0.000000e+00
4.18932640800e+06	2.603780e+03	0.000000e+00
4.45793672000e+06	2.448665e+03	0.000000e+00
4.74376972900e+06	2.302303e+03	0.000000e+00
5.04792971700e+06	2.163466e+03	0.000000e+00
5.37159176800e+06	2.032478e+03	0.000000e+00
5.71600631100e+06	1.908854e+03	0.000000e+00
6.08250395000e+06	1.795327e+03	0.000000e+00
6.47250060500e+06	1.689135e+03	0.000000e+00
6.88750298000e+06	1.585278e+03	0.000000e+00
7.32911438600e+06	1.490045e+03	0.000000e+00
7.79904093500e+06	1.399756e+03	0.000000e+00
8.29909813100e+06	1.315686e+03	0.000000e+00
8.83121788600e+06	1.235103e+03	0.000000e+00
9.39745597800e+06	1.159931e+03	0.000000e+00
1.00000000000e+07	1.090876e+03	0.000000e+00

"TRACE: B"
"FORMAT: LINEAR"

"Frequency"	"Data Trace Real"	"Data Trace Imag"
4.00000000000e+01	-6.158775e+01	0.000000e+00
4.25650000000e+01	-5.969400e+01	0.000000e+00
4.52940000000e+01	-5.951892e+01	0.000000e+00
4.81980000000e+01	-5.892480e+01	0.000000e+00
5.12880000000e+01	-5.763904e+01	0.000000e+00
5.45770000000e+01	-5.656187e+01	0.000000e+00
5.80760000000e+01	-5.499771e+01	0.000000e+00
6.18000000000e+01	-5.410530e+01	0.000000e+00
6.57620000000e+01	-5.346107e+01	0.000000e+00
6.99790000000e+01	-5.171681e+01	0.000000e+00
7.44660000000e+01	-5.048283e+01	0.000000e+00
7.92400000000e+01	-4.934726e+01	0.000000e+00
8.43210000000e+01	-4.830526e+01	0.000000e+00
8.97280000000e+01	-4.714801e+01	0.000000e+00
9.54810000000e+01	-4.598465e+01	0.000000e+00
1.01603000000e+02	-4.499522e+01	0.000000e+00
1.08117000000e+02	-4.313599e+01	0.000000e+00
1.15050000000e+02	-4.227554e+01	0.000000e+00
1.22426000000e+02	-4.093555e+01	0.000000e+00
1.30276000000e+02	-3.955367e+01	0.000000e+00
1.38629000000e+02	-3.791389e+01	0.000000e+00
1.47518000000e+02	-3.685694e+01	0.000000e+00
1.56976000000e+02	-3.619053e+01	0.000000e+00
1.67041000000e+02	-3.419640e+01	0.000000e+00
1.77751000000e+02	-3.293690e+01	0.000000e+00
1.89148000000e+02	-3.115575e+01	0.000000e+00
2.01276000000e+02	-3.100465e+01	0.000000e+00
2.14181000000e+02	-2.973040e+01	0.000000e+00
2.27914000000e+02	-2.861121e+01	0.000000e+00
2.42528000000e+02	-2.695969e+01	0.000000e+00
2.58078000000e+02	-2.600600e+01	0.000000e+00
2.74625000000e+02	-2.492718e+01	0.000000e+00
2.92234000000e+02	-2.358404e+01	0.000000e+00
3.10971000000e+02	-2.290882e+01	0.000000e+00
3.30910000000e+02	-2.198821e+01	0.000000e+00
3.52127000000e+02	-2.093758e+01	0.000000e+00
3.74705000000e+02	-1.928894e+01	0.000000e+00
3.98730000000e+02	-1.866654e+01	0.000000e+00
4.24296000000e+02	-1.815470e+01	0.000000e+00
4.51501000000e+02	-1.774771e+01	0.000000e+00
4.80450000000e+02	-1.712835e+01	0.000000e+00
5.11255000000e+02	-1.541495e+01	0.000000e+00
5.44036000000e+02	-1.491413e+01	0.000000e+00
5.78918000000e+02	-1.398248e+01	0.000000e+00
6.16037000000e+02	-1.341987e+01	0.000000e+00

6.55536000000e+02	-1.320259e+01	0.000000e+00
6.97567000000e+02	-1.272634e+01	0.000000e+00
7.42294000000e+02	-1.184614e+01	0.000000e+00
7.89888000000e+02	-1.133490e+01	0.000000e+00
8.40534000000e+02	-1.081967e+01	0.000000e+00
8.94427000000e+02	-1.048416e+01	0.000000e+00
9.51776000000e+02	-9.854602e+00	0.000000e+00
1.01280200000e+03	-9.655478e+00	0.000000e+00
1.07774000000e+03	-9.077223e+00	0.000000e+00
1.14684300000e+03	-8.989885e+00	0.000000e+00
1.22037600000e+03	-8.695431e+00	0.000000e+00
1.29862300000e+03	-7.821259e+00	0.000000e+00
1.38188800000e+03	-8.005996e+00	0.000000e+00
1.47049200000e+03	-7.315029e+00	0.000000e+00
1.56477600000e+03	-7.471416e+00	0.000000e+00
1.66510600000e+03	-7.014878e+00	0.000000e+00
1.77186900000e+03	-6.717301e+00	0.000000e+00
1.88547800000e+03	-6.579812e+00	0.000000e+00
2.00637000000e+03	-6.457429e+00	0.000000e+00
2.13501400000e+03	-6.086112e+00	0.000000e+00
2.27190700000e+03	-5.997662e+00	0.000000e+00
2.41757600000e+03	-5.802346e+00	0.000000e+00
2.57258600000e+03	-5.705904e+00	0.000000e+00
2.73753400000e+03	-5.547369e+00	0.000000e+00
2.91305900000e+03	-5.369897e+00	0.000000e+00
3.09983800000e+03	-5.264205e+00	0.000000e+00
3.29859300000e+03	-5.212102e+00	0.000000e+00
3.51009100000e+03	-5.172139e+00	0.000000e+00
3.73515000000e+03	-5.337987e+00	0.000000e+00
3.97464000000e+03	-5.122384e+00	0.000000e+00
4.22948500000e+03	-5.144008e+00	0.000000e+00
4.50067000000e+03	-5.195718e+00	0.000000e+00
4.78924300000e+03	-5.137596e+00	0.000000e+00
5.09631900000e+03	-4.932296e+00	0.000000e+00
5.42308400000e+03	-5.114136e+00	0.000000e+00
5.77080000000e+03	-5.324685e+00	0.000000e+00
6.14081000000e+03	-5.318532e+00	0.000000e+00
6.53454600000e+03	-5.422663e+00	0.000000e+00
6.95352600000e+03	-5.451693e+00	0.000000e+00
7.39937100000e+03	-5.698297e+00	0.000000e+00
7.87380200000e+03	-5.949716e+00	0.000000e+00
8.37865300000e+03	-5.954778e+00	0.000000e+00
8.91587300000e+03	-6.171119e+00	0.000000e+00
9.48753900000e+03	-6.190644e+00	0.000000e+00
1.00958590000e+04	-6.610971e+00	0.000000e+00
1.07431840000e+04	-6.875948e+00	0.000000e+00

1.14320130000e+04	-6.996816e+00	0.000000e+00
1.21650080000e+04	-7.377525e+00	0.000000e+00
1.29450010000e+04	-7.703309e+00	0.000000e+00
1.37750060000e+04	-7.989491e+00	0.000000e+00
1.46582290000e+04	-8.492931e+00	0.000000e+00
1.55980820000e+04	-8.907331e+00	0.000000e+00
1.65981960000e+04	-9.245995e+00	0.000000e+00
1.76624360000e+04	-9.577221e+00	0.000000e+00
1.87949120000e+04	-1.030243e+01	0.000000e+00
2.00000000000e+04	-1.066746e+01	0.000000e+00
2.12823560000e+04	-1.120861e+01	0.000000e+00
2.26469330000e+04	-1.166963e+01	0.000000e+00
2.40990040000e+04	-1.249100e+01	0.000000e+00
2.56441790000e+04	-1.307185e+01	0.000000e+00
2.72884270000e+04	-1.358352e+01	0.000000e+00
2.90381000000e+04	-1.429897e+01	0.000000e+00
3.08999580000e+04	-1.504689e+01	0.000000e+00
3.28811950000e+04	-1.600016e+01	0.000000e+00
3.49894650000e+04	-1.672382e+01	0.000000e+00
3.72329110000e+04	-1.765639e+01	0.000000e+00
3.96202030000e+04	-1.836861e+01	0.000000e+00
4.21605620000e+04	-1.938720e+01	0.000000e+00
4.48638040000e+04	-2.053251e+01	0.000000e+00
4.77403720000e+04	-2.146646e+01	0.000000e+00
5.08013780000e+04	-2.241150e+01	0.000000e+00
5.40586500000e+04	-2.363983e+01	0.000000e+00
5.75247710000e+04	-2.477774e+01	0.000000e+00
6.12131310000e+04	-2.600797e+01	0.000000e+00
6.51379810000e+04	-2.736474e+01	0.000000e+00
6.93144840000e+04	-2.869457e+01	0.000000e+00
7.37587750000e+04	-3.076243e+01	0.000000e+00
7.84880240000e+04	-3.208173e+01	0.000000e+00
8.35205020000e+04	-3.349601e+01	0.000000e+00
8.88756510000e+04	-3.539362e+01	0.000000e+00
9.45741610000e+04	-3.701929e+01	0.000000e+00
1.00638046000e+05	-3.802262e+01	0.000000e+00
1.07090734000e+05	-3.967243e+01	0.000000e+00
1.13957155000e+05	-4.214836e+01	0.000000e+00
1.21263834000e+05	-4.365421e+01	0.000000e+00
1.29039002000e+05	-4.503238e+01	0.000000e+00
1.37312697000e+05	-4.727702e+01	0.000000e+00
1.46116882000e+05	-4.878916e+01	0.000000e+00
1.55485573000e+05	-5.114838e+01	0.000000e+00
1.65454962000e+05	-5.275551e+01	0.000000e+00
1.76063567000e+05	-5.378998e+01	0.000000e+00
1.87352373000e+05	-5.567356e+01	0.000000e+00

1.99364991000e+05	-5.673888e+01	0.000000e+00
2.12147832000e+05	-5.811101e+01	0.000000e+00
2.25750280000e+05	-6.003332e+01	0.000000e+00
2.40224887000e+05	-6.124095e+01	0.000000e+00
2.55627573000e+05	-6.283750e+01	0.000000e+00
2.72017846000e+05	-6.410236e+01	0.000000e+00
2.89459027000e+05	-6.654319e+01	0.000000e+00
3.08018497000e+05	-6.768026e+01	0.000000e+00
3.27767960000e+05	-6.844503e+01	0.000000e+00
3.48783714000e+05	-6.971078e+01	0.000000e+00
3.71146951000e+05	-7.079236e+01	0.000000e+00
3.94944070000e+05	-7.133495e+01	0.000000e+00
4.20267008000e+05	-7.250051e+01	0.000000e+00
4.47213595000e+05	-7.365788e+01	0.000000e+00
4.75887939000e+05	-7.401371e+01	0.000000e+00
5.06400817000e+05	-7.531009e+01	0.000000e+00
5.38870114000e+05	-7.620164e+01	0.000000e+00
5.73421270000e+05	-7.694429e+01	0.000000e+00
6.10187769000e+05	-7.760011e+01	0.000000e+00
6.49311654000e+05	-7.818502e+01	0.000000e+00
6.90944077000e+05	-7.903621e+01	0.000000e+00
7.35245878000e+05	-7.975673e+01	0.000000e+00
7.82388212000e+05	-8.012397e+01	0.000000e+00
8.32553207000e+05	-8.064552e+01	0.000000e+00
8.85934671000e+05	-8.109997e+01	0.000000e+00
9.42738836000e+05	-8.147061e+01	0.000000e+00
1.00318515800e+06	-8.200075e+01	0.000000e+00
1.06750716400e+06	-8.242355e+01	0.000000e+00
1.13595335500e+06	-8.280795e+01	0.000000e+00
1.20878816300e+06	-8.318845e+01	0.000000e+00
1.28629297700e+06	-8.370207e+01	0.000000e+00
1.36876722800e+06	-8.388535e+01	0.000000e+00
1.45652954500e+06	-8.406834e+01	0.000000e+00
1.54991898800e+06	-8.432793e+01	0.000000e+00
1.64929635300e+06	-8.476886e+01	0.000000e+00
1.75504557500e+06	-8.505109e+01	0.000000e+00
1.86757520300e+06	-8.511148e+01	0.000000e+00
1.98731998000e+06	-8.542770e+01	0.000000e+00
2.11474252700e+06	-8.553587e+01	0.000000e+00
2.25033512500e+06	-8.577467e+01	0.000000e+00
2.39462161900e+06	-8.589900e+01	0.000000e+00
2.54815944300e+06	-8.605880e+01	0.000000e+00
2.71154177100e+06	-8.624978e+01	0.000000e+00
2.88539981200e+06	-8.640614e+01	0.000000e+00
3.07040524400e+06	-8.648448e+01	0.000000e+00
3.26727281500e+06	-8.659288e+01	0.000000e+00

3.47676309700e+06	-8.669264e+01	0.000000e+00
3.69968543000e+06	-8.672682e+01	0.000000e+00
3.93690105000e+06	-8.685658e+01	0.000000e+00
4.18932640800e+06	-8.683202e+01	0.000000e+00
4.45793672000e+06	-8.694839e+01	0.000000e+00
4.74376972900e+06	-8.697147e+01	0.000000e+00
5.04792971700e+06	-8.694539e+01	0.000000e+00
5.37159176800e+06	-8.693226e+01	0.000000e+00
5.71600631100e+06	-8.690345e+01	0.000000e+00
6.08250395000e+06	-8.682471e+01	0.000000e+00
6.47250060500e+06	-8.683527e+01	0.000000e+00
6.88750298000e+06	-8.686182e+01	0.000000e+00
7.32911438600e+06	-8.681261e+01	0.000000e+00
7.79904093500e+06	-8.682145e+01	0.000000e+00
8.29909813100e+06	-8.671078e+01	0.000000e+00
8.83121788600e+06	-8.664268e+01	0.000000e+00
9.39745597800e+06	-8.654452e+01	0.000000e+00
1.00000000000e+07	-8.597680e+01	0.000000e+00

APPENDIX B
SPECIFICATION INFORMATION FOR 42941A PROBE KIT

Up to 120 MHz (4-Terminal Pair): Probes

42941A Impedance probe kit

Terminal connector: 4-Terminal pair, BNC
Cable length (approx.): 1.5 m
Weight (approx.): 2400 g
Basic measurement accuracy: ±1%
For detailed information, refer to the operation manual or the specifications of E4990A-120.

E4990A-120 with 42941A

Open compensation

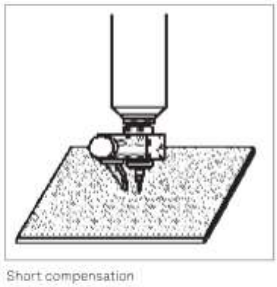

Short compensation

Description: This impedance probe kit is designed for use with the E4990A-120. It provides the capability to perform in-circuit measurements (printed circuit patterns, the input/output impedance of circuits, etc.) with better accuracy and wider impedance coverage from 20 Hz to 120 MHz. DUTs can be connected by either using the pin probe, the clip lead (alligator clip adapter) or the BNC adapter. All probe adapter can be used from 20 Hz to 120 MHz. The pin probe is best for in-circuit, board-mounted components, The clip lead is for components too large for the pin probe. The BNC adapter is used to connect circuits or networks equipped with BNC connectors.
Applicable instrument: E4990A-120
Frequency: 20 Hz to 120 MHz
Maximum voltage: ±42 V peak max. (AC+DC)
Operating temperature: –20 to +75°C (probe only)
Furnished accessories:

Description	P/N	Qty.
Pin probe	42941-60002	1
Adapter BNC-SMA	1250-2375	1
Spare pin Set (3 ea.)	42941-60004	1
3.5 mm SHORT	1250-2840	1
3.5 mm LOAD	0955-1105	1
Clip lead	8121-0003	1
Ground lead	04193-61679	1
Carrying case	42941-60011	1
Operating and service manual	42941-90010	1

Compensation and measurement: Adapter setup and compensation is required before measurement. In the Adapter setup menu, select PROBE 42941A. Use the furnished 3.5 mm short and load standards. The open condition can be created by not connecting the probe to anything. Perform phase compensation, short and load data measurements. For compensation, open and short compensation is recommended. Short compensation is performed by shorting the probe. To short the probe it is recommended to use a shorting device with gold-plated surfacing (which provides stable contact resistance).

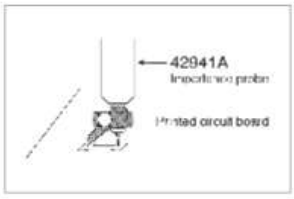

In-circuit measurement

APPENDIX C

SPECIFICATION INFORMATION FOR 4294A PRECISION IMPEDANCE ANALYZER

Agilent 4294A

Precision Impedance Analyzer
40 Hz to 110 MHz

Technical Overview

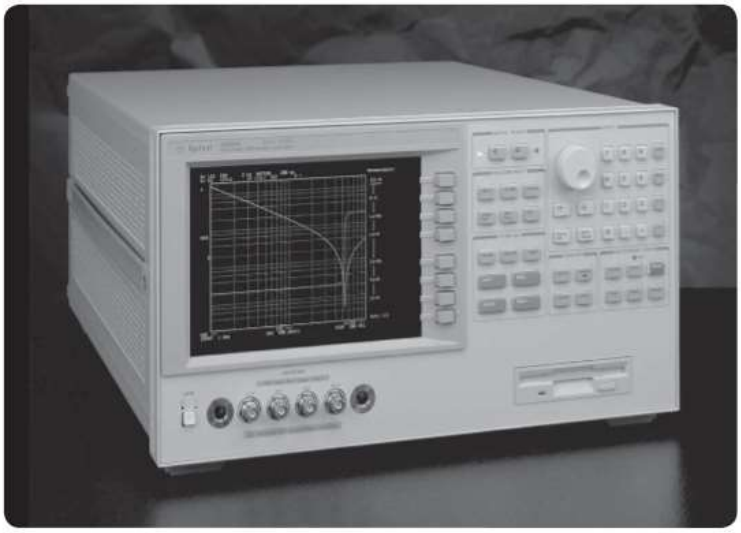

New generation precision impedance analyzer for functionality and efficiency in engineering

Agilent Technologies

Agilent 4294A Precision Impedance Analyzer

The Agilent Technologies 4294A precision impedance analyzer greatly supports accurate impedance measurement and analysis of a wide variety of electronic devices (components and circuits) as well as electronic and non-electronic material.

- **Accurate measurement over wide impedance range and wide frequency range**
- **Powerful impedance analysis functions**
- **Ease of use and versatile PC connectivity**

8.5 inch TFT color display. **Powerful analysis tools available. 801 sweep points, 4 traces (2 data traces and 2 memory traces), 8 markers, marker analysis functions, and equivalent circuit analysis function.**

User-friendly interface. **Based on Agilent's widely accepted user-interface.**

Rigid fixture/accessory connection. **Provides highly repeatable and reliable measurements.**

IBASIC programming function. **Automatic set up, measurement, and computation as well as remote instrument control is possible.**

Built-in 10 Mbyte nonvolatile memory. **Data or setup files can be quickly saved or recalled.**

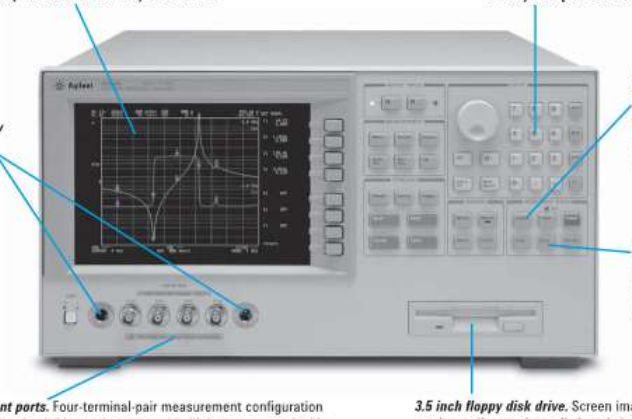

Impedance measurement ports. Four-terminal-pair measurement configuration and the newest auto-balancing bridge technique enable high accuracy and wide impedance range.

3.5 inch floppy disk drive. Screen images, data and setup files can be easily saved, recalled, and shared (1.44 Mbyte).

Two digital I/O ports.
Control other instrument(s) or use an external controller (instrument or computer) via 8 bit or 24 bit programmable I/O port.

External VGA Output.
Display measurements on a large VGA monitor. Reduces eyestrain, improves team work and communication.

LAN Interface (10 Base-T)
Another instrument control method or simplified file sharing.

GPIB Interface. Automatic measurement system is easily configured with an external instrument or computer.

External keyboard Interface. Makes IBASIC program development easier (mini DIN keyboard).

Printer (Centronics) Interface. Connects PCL3 printers directly to the instrument.

40 Hz to 110 MHz

The Agilent 4294A is a powerful tool for design, qualification, quality control, and production testing of electronic components. Circuit designers and developers can also benefit from the performance/functionality offered.

Moreover, the 4294A's high measurement performance and capable functionality delivers a powerful tool to circuit design and development as well as materials research and development (both electronic and non-electronic materials) environments.

The following are application examples:

Electronic devices

Passive component

- Impedance measurement of two terminal components such as capacitors, inductors, ferrite beads, resistors, transformers, crystal/ceramic resonators, multi-chip modules or array/network components.

Semiconductor components

- C-V characteristic analysis of varactor diodes.
- Parasitic analysis of a diode, transistor, or IC package terminal/leads.
- Amplifier input/output impedance measurement.

Other components

- Impedance evaluation of printed circuit boards, relays, switches, cables, batteries, etc.

Materials

Dielectric material

- Permittivity and loss tangent evaluation of plastics, ceramics, printed circuit boards, and other dielectric materials.

Magnetic material

- Permeability and loss tangent evaluation of ferrite, amorphous, and other magnetic materials.

Semiconductor material

Permittivity, conductivity, and C-V characterization of semiconductor materials.

Agilent 4294A key specifications

Operating frequency	40 Hz to 110 MHz, 1 mHz resolution
Basic impedance accuracy	±0.08%
Q accuracy	±3% (typical) @ Q = 100, f ≤ 10 MHz
Impedance range	3 mΩ to 500 MΩ*1
Measurement time	3 msec/point @ f ≥ 500 kHz, BW = 1 (fast)
Number of points per sweep	2 to 801 points
Measurement type	Four-terminal-pair measurement (standard)
	7-mm one port measurement (with the 42942A) measurable grounded devices
	Impedance probe measurement (with the 42941A) measurable grounded devices
Impedance parameters	IZI, IYI, θ, R, X, G, B, L, C, D, Q
DC bias	0 to ±40 V/100 mA, 1 mV/40 µA resolution
	Constant voltage/constant current mode, DC bias V/I monitor function
OSC level	5 mV to 1 Vrms/200 µA to 20 mArms OSC level V/I monitor function
Sweep parameter	Frequency, OSC level (V/I), DC bias (V/I)
Sweep type	Linear, log, list: manual sweep mode: up/down sweep
Other function	Equivalent circuit analysis function, Limit line function
	Trace accumulate mode
Marker	Eight markers (one main marker and seven sub markers)
	Delta marker function, marker search function (Max, Min, Peak, Next peak, etc.)
	Marker analysis function

(*1) 30% typical accuracy range: 3 mΩ (100 Hz to 110 MHz), 500 MΩ (100 Hz to 200 kHz)

Accurate, Real-World Characterization of Electronic Components

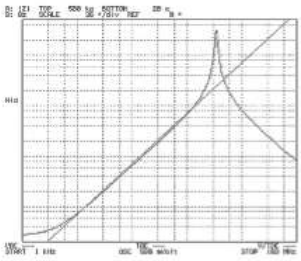

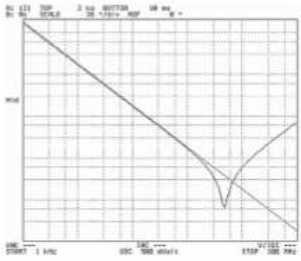

There is no ideal inductor (L), capacitor (C), or resistor (R). In reality, operating conditions such as signal level and frequency determine the real-world performance of a device based on the electronic characteristics of the device. An ideal component of high quality could be considered to possess a single, perfect circuit element over some frequency range. However, in reality, most components will resonate as shown in these figures as the frequency increases.

This is due to the fact that there are both capacitive and inductive elements present in real world components. Component characteristics cannot be expressed correctly with a two-element model when the model contains only one single reactive element. The Agilent 4294A equivalent circuit function enables modeling of the impedance vs. frequency characteristics with three or four elements. This function helps you design quality circuits and effective components.

Equivalent circuit analysis

The equivalent circuit function is used to fit a circuit model to measured data, or to simulate device performance based on the value of each circuit model element.

The 4294A has been programmed with five equivalent circuit models to choose from. This function automatically extracts equivalent circuit parameters from actual measurement data. The characteristics of the device under test (DUT) or the material under test (MUT) can be analyzed with extracted model element values.

NOTE: The simulation result and the actual measurement data can be displayed on the same screen.

Step 1.
After taking a measurement,

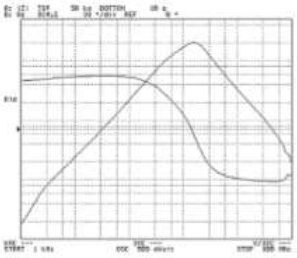

Step 2.
select an appropriate circuit model

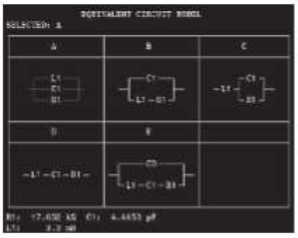

Step 3.
and extract the circuit model parameters.

Step 4.
Then compare the simulation to the actual measurement data. If the data does not match, select a different equivalent circuit model and try again.

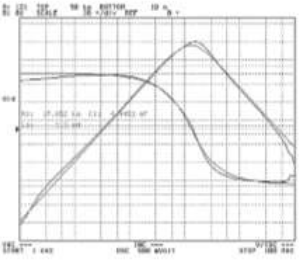

State-of-the-art technology for improved measurement performance

The Agilent 4294A employs a state-of-the-art auto-balancing-bridge technique in a four-terminal-pair (4TP) measurement configuration. Meticulous circuit design against distortion and instability resulted in a highly accurate and stable measurement system for a wide impedance range.

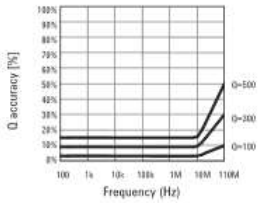

4294A Q accuracy (typical)
OSC level = 250 mV

For evaluation of low-loss devices

With the trend toward lower power consumption and compact equipment, inductors and capacitors are becoming smaller with lower loss. The efficiency improvement in power conversion for switching power supply applications is an example. These applications require low-loss induc-tors and capacitors.

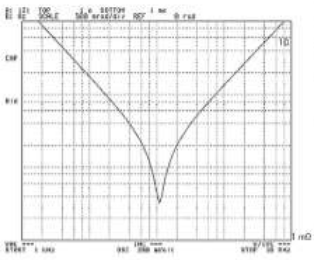

Low-loss capacitor ESR (equivalent series resistance) measurement (100 µF ceramic C)

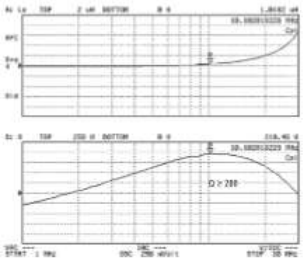

High Q inductor measurement (low-loss)

For evaluating devices with wide impedance range

A wide impedance range is required to accurately measure both resonant impedance and anti-resonant impedance of crystal/ceramic resonators.

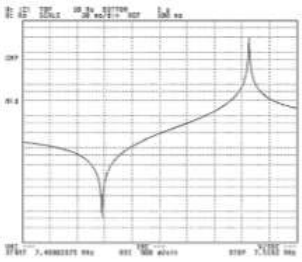

Crystal resonator impedance measurement

The 4294A covering several decades (mΩ to hundreds of MΩ) of impedance can measure resonator characteristics accurately.

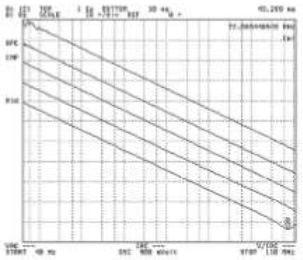

SMD capacitor impedance measurement (using the 42942A)

The dynamic range of the 4294A in terms of impedance is more than 200 dB. When compared to that of a general network analyzer with a direc-tional bridge, at 80 dB, it is clear, the 4294A has an extremely broad impedance-measurement range.

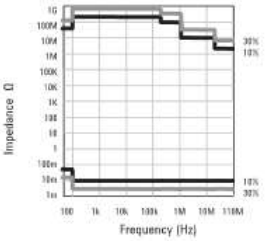

Impedance measurement range (typical)

Impedance Analysis Under Various Operating Conditions

Signal level dependency

The impedance characteristics of some devices change drastically as a function of the signal level. The Agilent 4294A can sweep test signal voltage, 5 mVrms to 1 Vrms (1 mV resolution), or test signal current 200 µArms to 20 mArms (20 µA resolution) to evaluate signal level dependency.

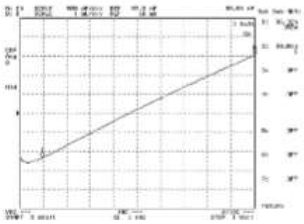

Signal level dependency of a ceramic capacitor with high permittivity (signal-level swept from 5 mV to 1 V, 0.1 µF capacitor at 1 kHz)

DC level dependency

The DC component of an applied signal often affects device impedance. The 4294A can sweep either the DC voltage bias from –40 V to +40 V (with 1 mV resolution) or the DC current bias from –100 mA to +100 mA (with 40 µA resolution) to evaluate DC signal dependency. This capability also empowers analysis of the DC-voltage bias dependency for C-V characterization of varactor diodes or other DC-voltage bias dependent devices. The DC level dependency figure shows an example of varactor diode measurement.

The DC bias auto level control (ALC) function, based on a feedback loop technique, accurately maintains the applied DC voltage bias or current bias. While the impedance of a device might change during a sweep, this ALC function insures that the signal level setting is the actual signal level applied to the DUT.

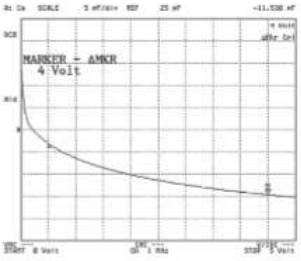

Varactor diode capacitance vs. DC voltage characteristic. DC bias sweep from 0 V DC to 5 V DC. f = 1 MHz

Efficient analysis with the list sweep function

The list sweep function enables different measurement setups in a single sweep by dividing the sweep range into segments. The measurement setup, including the frequency range, averaging time, measurement bandwidth, test signal level (V or A), and DC bias can be different for each segment. The frequency range of each segment can be continuous, separated, or overlapped.

Evaluation of a crystal resonator requires that the nominal resonant frequency, the nominal anti-resonant frequency, and some spurious frequencies be determined. These parameters can be efficiently measured by setting an appropriate frequency range for each segment.

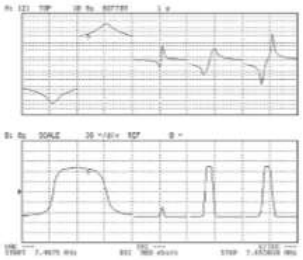

Crystal resonator evaluation by list sweep function

SEG	START	STOP	NOP	OSC	BIAS	IM	AVG
1	7.49750MHz	7.49988MHz	81	500mV	0V	3	1
2	7.51355MHz	7.51405MHz	20	500mV	0V	3	1
3	7.53963MHz	7.54063MHz	20	500mV	0V	3	1
4	7.60035MHz	7.61035MHz	20	500mV	0V	3	1
▸ 5	7.64304MHz	7.65304MHz	20	500mV	0V	3	1

Edit screen of list sweep

Powerful functions for efficient evaluation

Sweep, display, and markers

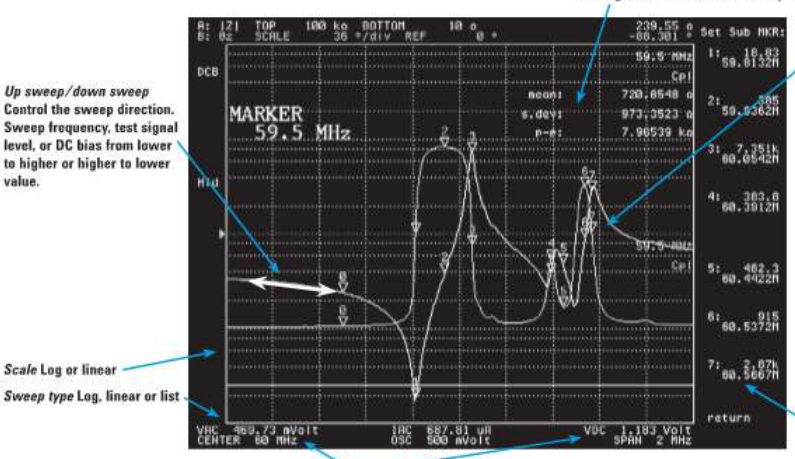

Three multi-trace modes for comparison evaluation

Superimpose trace (accumulate) mode
This mode is used to observe an inter-mittent event or a change in the characteristic performance of a device over time.

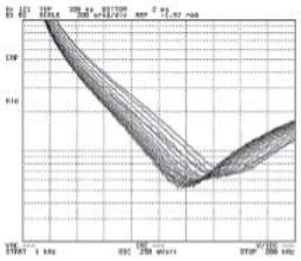

Accumulation of resonance vs. temperature data for a ceramic capacitor

List sweep mode
Superimpose and compare measurement data on the same display by setting the list sweep segments to the same frequency range with different DC bias or test signal levels. Markers can be used on each trace.

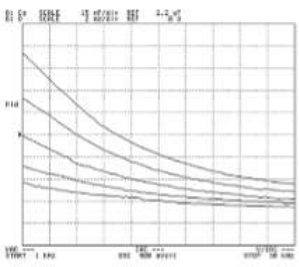

Capacitance variations of ceramic capacitor (2.2 µF) with high permittivity measured by stepping the test signal level from 0.1 V to 0.9 V in 0.2 V steps (five list sweep segments)

Data/Memory trace
A data trace and a memory trace are available at each channel. The underlying data can be saved as the memory trace. Some simple calculations are possible with data math functions.

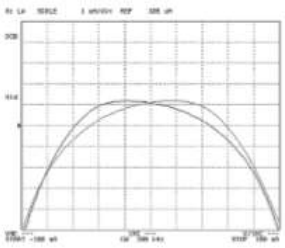

Inductor DC dependency characteristics (100 µH inductor at 100 kHz) UP and DOWN DC current bias sweep from –100 mA to +100 mA. Hysteresis is observed.

7

Easy, automatic measurement system configurations

Labs today often require system configurations in which test instruments interact with other instruments or handshake with external computers.

Agilent 4294A functions that support efficient systems:

- Instrument BASIC programming function for automatic measurement or external measurement instrument control without an external computer.
- List Sweep function for measuring only at desired points.
- Limit line function for Go/NoGo testing.
- Built-in 10 Mbyte non-volatile memory to quickly save/recall data/setup.
- Two types programmable digital I/O port (24 bit and 8 bit) for data transfer with external device such as sensor, and for external device control.
- LAN interface for networking with computers.

The LAN I/F dramatically expands the ability to share files, data, or instrument control. Measurement setup, result, and graphics files can be transferred via FTP (File Transfer Protocol) to or from the instrument.

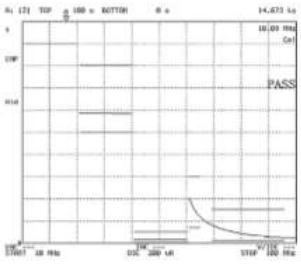

Limit test
Limit test of PIN diode impedance. 4 segment list sweep with different DC bias voltages and different frequency ranges using constant DC bias voltage (ALC) mode.

Agilent 4294A interfaces

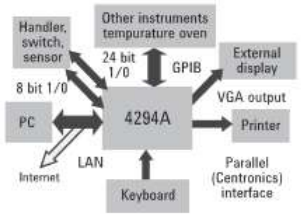

IBASIC programming function
Instrument BASIC (IBASIC) is a programming language developed from BASIC programming language. The keystroke recording function helps to easily develop automatic measurement program with front panel keys. When a key is pressed, the GPIB command corresponding to the key is automatically recorded in the program. Writing or editing programs the old-fashioned way is made easier with the mini-DIN key board.

One touch IBASIC program execution
When you press the softkey with the file name of an IBASIC program saved in either internal memory or floppy disk, the program is automatically downloaded and executed. Once customized IBASIC programs are developed, quick measurement and data analysis is possible because each program works as if it is a built-in function.

A feature with high visibility
The Agilent 4294A has VGA output on the rear panel. Automatic test or component adjustment in production line or QA test can easily be performed with a large external monitor.

Accessories for various measurement needs

Agilent 42941A impedance probe

The 42941A impedance probe enables in-circuit impedance measurement of electronic circuits or components. Grounded devices can also be measured.

Key specifications
Frequency: 40 Hz to 110 MHz
DC BIAS: 0 V to ±40 V
Operation temperature range:
–20 °C to 75 °C
Basic impedance accuracy: ±0.8%

Agilent 42942A terminal adapter

The 42942A terminal adapter converts the four-terminal-pair port configuration to an 7-mm port. This adapter permits the use of familiar 7-mm test fixtures.

Again, grounded measurement is available.

Key specifications
Frequency: 40 Hz to 110 MHz
DC bias: 0 V to ±40 V
Operation temperature range:
0 °C to 40 °C
Basic impedance accuracy: ±0.6%

Material test fixtures

Use of a dielectric material fixture such as the Agilent 16451B or 16452A allows accurate dielectric material measurement. Permeability of magnetic materials can also be evaluated with the Agilent 42942A and 16454A magnetic material test fixture. Automatic measurement and permittivity/permeability analysis can easily be performed by using built-in IBASIC or by I/0 to a computer where the analysis can be performed.

Other accessories
When a DUT cannot be positioned near the instrument, a four-terminal-pair extension (Agilent 16048G: 1 m or 16048H: 2 m) can be used to extend the test station to the DUT. These Agilent extension accessories operate over the entire frequency and temperature range (40 Hz to 110 MHz, –20 °C to +150 °C) of the 4294A.

Ordering Information

Agilent 4294A precision impedance analyzer

Accessories included:

- 100 Ω load resistor for four-terminal-pair extension
- Sample program disk
- Power cable

Options:

- **4294A-800** Standard frequency reference
- **4294A-810** Add mini DIN keyboard
- **4294A-1D5** High-stability frequency reference
- **4294A-ABA** English localization
- **4294A-ABJ** Japanese localization
- **4294A-0BW** Add service manual
- **4294A-1A7** ISO 17025 compliant calibration
- **4294A-1CM** Rack mount kit
- **4294A-1CN** Front handle kit
- **4294A-1CP** Rack mount and front handle kit

Accessories available:

- **Four-terminal-pair test leads (16048G/16048H)**

1 m/2 m four-terminal-pair port extension cable with BNC connectors.
Frequency: 40 Hz to 110 MHz
DC bias: 0 V ±40 V
Operation temperature range:
–20 °C to 150 °C
Cable length: 1 m (16048G)
2 m (16048H)

Accessories available:

- **42941A impedance probe kit**

Convert four-terminal-pair port configuration to a one-port probe.

Furnished items:

- Probe and Four-terminal Pair Connection Block
- Pin probe
- Spare pin set (includes 3 spare pins)
- 3.5 mm SHORT
- 3.5 mm LOAD (50 Ω)
- BNC adapter
- Clip lead
- Ground lead
- Carrying case
- Operation and Service Manual

42941A Impedance probe kit

Impedance probe with connection block

Agilent 42942A terminal adapter

Converts four-terminal-pair port configuration to an APC-7 port.

Furnished items

- Terminal adapter
- 7 mm OPEN*
- 7 mm SHORT*
- 7 mm LOAD (50 Ω)*
- Operation and Service Manual

* Furnished with Option 42942A-700

Option:

42942A-700 Add 7 mm open/short/load set

Items included:

- 7 mm open reference
- 7 mm short reference
- 7 mm 50 Ω reference
- Operating manual/data sheet

42942A Terminal adapter (set) including option 42942A-700

Terminal adapter

Fixtures

Fixtures for leaded components

16047E (DC to 110 MHz)
For leaded components. This fixture features the capability to clamp the leads between the electrodes and adjust the pressure. A guard terminal is provided for three port device measurements.

Accessories provided:
Shorting plate
4294A mounting tool

16047A/D (DC to 3 MHz/40 MHz)
For leaded components. These fixtures use spring actuated clamps to hold device leads.

16092A (DC to 500 MHz)
For leaded or surface mount (SMD) components. Attachments for leaded or SMD are provided. Note: The 42942A adapter is required.

16093-65003/4 (DC to 250 MHz)
This is a binding post type fixture.
Note: The 42942A adapter is required.

Fixtures for SMD

16034G (DC to 110 MHz)
0201 (0603) to 1206 (3216) size components. Maximum dimensions: 5 mm (L) x 1.6 mm (W) x 1.6 mm (H)

16034E (DC to 40 MHz)
0603 (1608) or larger size components can be measured. Maximum dimensions: 8 mm (L) x 10 mm (W) x 10 mm (H)

16196A/B/C/D (DC to 3 GHz)
Coaxial fixture specialized for the following SMD sizes:
16196A: 1608 (0603)
16196B: 1005 (0402)
16196C: 0603 (0201)
16196D: 0402 (01005)
Note: The 42942A adapter is required

16044A (DC to 10 MHz)
Features a Kelvin connection suitable for low impedance measurement of 0603 (1608) size components or larger. Maximum dimensions: 8 mm (L) x 8 mm (W) x 3 mm (H)

16197A (DC to 3 GHz)
These fixture is for bottom electrode components. Applicable size is 0201 (0603) to 1210 (3225).
Note: The 42942A adapter is required.

* Option 16197A-001 is required for 0201 inch/0603 mm.

16192A (DC to 2 GHz)
This fixture uses side electrode contacts 0603 (1608) or larger size components. Note: The 42942A adapter is required.

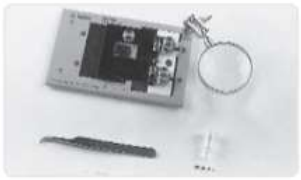

Material test fixtures

16451B
A dielectric material test fixture, with parallel plate electrodes.

16452A (20 Hz to 30 MHz)
Dielectric test fixture for liquid material.

16454A (1 MHz to 1 GHz)
Fixture for troidal magnetic material.
Note: The 42942A adapter is required.

Special purpose accessories

16065A (50 Hz to 2 MHz)
External DC bias adapter to ±200 V
Note: For leaded components.

Web Resource

www.agilent.com/find/impedance

Remove all doubt

Our repair and calibration services will get your equipment back to you, performing like new, when promised. You will get full value out of your Agilent equipment throughout its lifetime. Your equipment will be serviced by Agilent-trained technicians using the latest factory calibration procedures, automated repair diagnostics and genuine parts. You will always have the utmost confidence in your measurements. For information regarding self maintenance of this product, please contact your Agilent office.

Agilent offers a wide range of additional expert test and measurement services for your equipment, including initial start-up assistance, onsite education and training, as well as design, system integration, and project management.

For more information on repair and calibration services, go to:

www.agilent.com/find/removealldoubt

Product specifications and descriptions in this document subject to change without notice.

Agilent Email Updates

www.agilent.com/find/emailupdates
Get the latest information on the products and applications you select.

Agilent Direct

www.agilent.com/find/agilentdirect
Quickly choose and use your test equipment solutions with confidence.

www.agilent.com

For more information on Agilent Technologies' products, applications or services, please contact your local Agilent office. The complete list is available at:

www.agilent.com/find/contactus

Americas

Canada	(877) 894-4414
Latin America	305 269 7500
United States	(800) 829-4444

Asia Pacific

Australia	1 800 629 485
China	800 810 0189
Hong Kong	800 938 693
India	1 800 112 929
Japan	0120 (421) 345
Korea	080 769 0800
Malaysia	1 800 888 848
Singapore	1 800 375 8100
Taiwan	0800 047 866
Thailand	1 800 226 008

Europe & Middle East

Austria	01 36027 71571
Belgium	32 (0) 2 404 93 40
Denmark	45 70 13 15 15
Finland	358 (0) 10 855 2100
France	0825 010 700* *0.125 €/minute
Germany	07031 464 6333
Ireland	1890 924 204
Israel	972-3-9288-504/544
Italy	39 02 92 60 8484
Netherlands	31 (0) 20 547 2111
Spain	34 (91) 631 3300
Sweden	0200-88 22 55
Switzerland	0800 80 53 53
United Kingdom	44 (0) 118 9276201

Other European Countries:
www.agilent.com/find/contactus

Revised: October 1, 2008

Printed in USA, November 13, 2008
5968-3808E

Agilent Technologies

APPENDIX D

SPECIFICATION INFORMATION FOR 8W20IDF PET

Electrodes per Well	Electrode Area (mm^2)	Maximum Number of Cells Measured	Well Volume (µL)
idf	3.985	4000-8000	600

Each of the 8 wells has a total electrode area of 3.985mm^2 located on inter-digitated fingers to provide measurements of cells. Each well has a substrate area of 0.8cm^2 and a maximum volume of 600 µL. On average, with a confluent layer, approximately 4000 to 8000 cells will be measured by the electrodes.

The 8W20idf PET arrays are designed to monitor larger numbers of cells, sampling over the entire bottom of the well. Because of the relatively high number of cells, impedance fluctuations due to micromotion are smoothed out and do not obscure subtle changes in impedance due to the experimental conditions.

Applications include:

- *Cell Attachment and Spreading*
- *Cell proliferation*
- *Cytotoxicity*

CURRICULUM VITA

Margaret Jett
Local: 1312 S 6th St, Apt 1, Louisville, KY, 40208
Phone: 513-267-6288 **Email:** mrjett001@gmail.com

EDUCATION

Bachelor of Science in Mechanical Engineering May 2018
University of Louisville, Louisville, Kentucky GPA 3.8/4.0
Master of Engineering August 2021
University of Louisville, Louisville, Kentucky GPA 3.3/4.0

WORK EXPERIENCE

University of Louisville, Research Assistant January 23, 2019 – July 20, 2019

Michelin, Reliability August 15, 2016 – December 16, 2016; May 15, 2017- August 11, 2017

Michelin, Quality January 11, 2016 - May 9, 2016

PUBLICATIONS

MR Jett, MZ Rashed, SP Hendricks, and SJ Williams, "Electrical characterization of phytoplankton suspensions using impedance spectroscopy," Journal of Applied Phycology, 33, 1643-1650 (2021).

AWARDS

Mechanical Engineering Department Sophomore Academic Achievement Award 2015

PRESENTATIONS

MR Jett, K Henson, MZ Rashed, S Hendricks, and SJ Williams, "Impedance spectroscopy based evaluation of phytoplankton health," 2019 Colloid & Surface Science Symposium, Atlanta, GA, June 16-19, 2019. (Poster)

MR Jett, KM Henson, MZ Rashed, SP Hendricks, and SJ Williams, "Impedance spectroscopy based evaluation of phytoplankton health," Kentucky Water Resources Annual Symposium, Lexington, KY, March 23, 2019 (Poster).